UNIVERSITY OF BEIRA INTERIOR
Engineering

Modeling of an Autonomous Underwater Vehicle

Cristiano Alves Bentes

Thesis submitted in fulfillment of Master Degree in
Aeronautical Engineering
(Integrated Cycle of Studies)

Academic Supervisor: Professor Kouamana Bousson

Covilhã, October 2016

Dedication

To my parents, Maria Fernanda Veigas Alves and João Jaime Bentes, for all the support and dedication.

To my family and friends who have always been there for me.

”My momma always said, ”Life was like a box of chocolates. You never know what you’re gonna get.””

-Forrest Gump

Acknowledgments

Thank you to my academic supervisor Professor Kouamana Bousson for all the dedication and support.

My utmost gratitude to my co-supervisor, Tiago Rebelo, and all the engineers at CEiiA, who provided much needed guidance and support during my internship.

My absolute gratitude to my parents, Fernanda and João, for their unconditional love and support.

A special thanks Maria, Lucy and Serra, for their friendship.

Finally, thank you to those who made this work possible and those guided me along the way.

Resumo

Os veículos subaquáticos autónomos (*Autonomous Underwater Vehicles* – AUV's) têm múltiplas aplicações militares, comerciais e para investigação científica. A grande vantagem destes veículos advém da sua independência, sendo que operam sem a necessidade de supervisão humana. No entanto esta capacidade implica que os sistemas de navegação, guia e controlo sejam completamente responsáveis pelo governo do veículo. O sistema de controlo destes veículos é tipicamente projetado tendo como base um modelo dinâmico do mesmo. Este modelo pode ser também usado para simulação e análise de desempenho. O propósito deste trabalho é desenvolver um modelo dinâmico para um AUV de investigação de duplo-corpo, a ser desenvolvido no CEiiA.

Dado que o objetivo principal do modelo é projetar controladores e, de modo a fornecer várias abordagens para o efeito, os respetivos modelos (subsistemas) lateral e longitudinal são deduzidos. Estes modelos são posteriormente validados através da comparação de resultados de simulação para os subsistemas com os resultados de simulação para o modelo completo.

A modelação deste veículo é efetuada usando o modelo dinâmico de Fossen. Este modelo pode ser dividido em *cinemática* e *cinética*. Cinemática aborda os aspetos geométricos do movimento. As equações de cinemática são fornecidas tanto para ângulos de Euler como para quaterniões. As equações de cinética centram-se na relação entre movimento e força. O modelo de Fossen identifica quatro forças distintas que influenciam a dinâmica dos veículos subaquáticos: forças de corpo rígido; forças hidrostáticas; amortecimento (atrito) hidrodinâmico e *added mass*. Estas forças são modeladas através de métodos analíticos e computacionais. O modelo CAD do veículo, desenvolvido pelo CEiiA, foi usado para estimar os parâmetros de massa e inércia, bem como forças hidrostáticas. O amortecimento hidrodinâmico foi estimado através da adaptação de análises CFD, também efetuadas pelo CEiiA, para satisfazer os parâmetros do modelo. Os parâmetros *added mass* foram estimados usando métodos analíticos comprovados. Devido a limitações inerentes aos métodos de modelação atuais, simplificações foram inevitáveis. As mesmas, quando analisadas tendo em conta os requisitos de sistemas de controlo típicos não provaram ser impeditivas da aplicação deste modelo para o desenvolvimento dos mesmos. No que diz respeito à dinâmica deste AUV, a análise hidrodinâmica sugere que este AUV é instável quando na presença de ângulos de ataque e derrapagem. No entanto os motores do AUV deverão ser capazes de corrigir tais instabilidades.

Palavras-chave

Veículo Subaquático autónomo; Duplo-corpo; Dinâmica; Estimação; Modelo de Fossen; Lateral; Longitudinal; Simulação.

Abstract

Autonomous Underwater Vehicles (AUV) have multiple applications for military, commercial and research purposes. The main advantage of this technology is its independence. Since these vehicles operate autonomously, the need for a dedicated support vessel and human supervision is dismissed. However, the autonomous nature of AUVs also presents a complex challenge for the guidance, navigation and control system(s). The design of motion controllers for AUVs is model-based i.e. a dynamic model is used for the design of the control system. The dynamic model can also be used for simulation and performance analysis. In this context, the purpose of this thesis is to provide a dynamic model for a double-body research AUV being developed at CEiiA. This model is to be subsequently used for the design of the control system.

Since the purpose is the design of the control system and, in the scope of providing multiple design approaches, the appropriate lateral and longitudinal subsystems are devised. These subsystems are subsequently validated by comparing simulation results for the subsystems with simulation results for the complete model.

The AUV is modeled using Fossen's dynamic model. The model is divided into *kinematics* and *kinetics*. Kinematics addresses the geometrical aspects of motion. For this purpose, both Euler angles and quaternions are used. Kinetics focuses on the relationship between motion and force. This model identifies four distinct forces that act on the underwater vehicle: rigid-body forces; hydrostatic forces; hydrosynamic damping (or drag) and added-mass. The estimation of model parameters is performed using analytical and computational methods. A detailed 3D CAD model, developed by CEiiA, proved helpful for estimating mass and inertia parameters as well as hydrostatic forces. Hydrodynamic damping estimation was performed by adapting CFD analysis, also developed by CEiiA, to satisfy model parameters. Added mass parameters were estimated using proven analytical methods. Due to limitations inherent to current modeling methods, simplifications were unavoidable. These, when analyzed considering the requirements of typical control systems, did not pose an impediment to the use of the dynamic model for this purpose. Regarding the dynamics of this AUV, the hydrodynamic analysis suggests that this AUV is unstable in the presence of angles of attack and side-slip. However the AUV's motors should be capable of controlling such instabilities.

Keywords

Autonomous Underwater Vehicle; Double-body; Dynamics; Estimation; Fossen's model; Lateral; Longitudinal; Simulation.

Contents

List of Figures

List of Tables

LIST OF TABLES

List of Acronyms

2D	Two Dimensions
3D	Three Dimensions
AUV	Autonomous Underwater Vehicle
CAD	Computer-Aided Design
CB	Center of Buoyancy
CEiiA	Centro de Engenharia e Desenvolvimento de Produto
CFD	Computational Fluid Dynamics
CG	Center of Gravity
DNV GL	Det Norske Veritas Germanischer Lloyd
DoF	Degree of Freedom
DVL	Doppler Velocity Log
NED	North-East-Down
ECEF	Earth-Centered Earth-Fixed
GC	Geometric Center
GPS	Global Positioning System
INS	Inertial navigation system
LBC	Lower Body Center
NDD	Nominal Diving Depth
PID	Proportional–Integral–Derivative
ROV	Remotely Operated Vehicle
SNAME	Society of Naval Architects and Marine Engineers
UBI	University of Beira Interior (EN)
UBL	Upper Body Center
US	United States
UUV	Unmanned Underwater Vehicle

LIST OF TABLES

Chapter 1

Introduction

The ocean has been a source of valuable resources throughout human history. Although humans have ”sailed the seven seas” and actively exploited this mean for resources, our knowledge of the underwater environment remains limited. Extreme pressures, high corrosion, low visibility, limitations in underwater communications, difficult access and unstable environmental conditions are few reasons that make the ocean a difficult medium to explore. Ever since the first ships sailed towards the unknown that these challenges are a source of great mythical fears, as found in popular literature like *Os Lusíadas* by portuguese poet *Luís de Camões*. Nowadays, superstition has given place to science, but the challenges for marine exploration remain.

Remotely Operated Vehicles (ROVs) have been the workhorse of underwater exploration. ROVs maintain communication and receive power via a umbilical-tether between the vehicle and a dedicated support vessel. A skilled operator is often required to control the craft. The need for a dedicated support vessel and a skilled operator translates into high operational costs. Recently, modern technology, most notably in computer science, allowed the advent of the Autonomous Underwater Vehicle (AUV). AUVs, like ROVs, are a type of Unmaned Underwater Vehicle (UUV)[1]. The AUV operates autonomously, meaning that the AUV’s mission has to be pre-programmed before its deployment. Since no physical link is present between the vehicle and the support vessel, the risk of vehicle loss is substantial, thus, assuring survivability is a complex, multi-variable task. The independence of AUV is, at the same time, the greatest advantage and disadvantage of these systems.

Presently, ocean exploration is a subject of great interest for military, economic and scientific purposes. These are the main sources of applications for AUVs. Versatility and independence makes the AUV a useful tool capable of addressing current needs. Either for cost reduction or increased capability, the interest for the technology certainly exists [2, 3]. The military sector was the first to experiment with AUVs, during the 1960’s. Sumbarine launched nuclear ballistic missiles is one, probably the most worrying, of many marine threats in the case of war. The AUV can be used to conteract such threats and provide unprecedented millitary capability [4]. Today, the millitary sector is still the most significant client in the AUV market. Academic organizations also started developing AUVs aimed for specific scientific studies. In the last decade, the use of AUVs to collect data led to major advances in oceanography. Such studies allow humans to obtain valuable knowledge about the natural laws and forces that govern our oceans [5]. The use of AUVs remained limited to the public sector until the oil & gas industry showed interest in the technology for cost reduction purposes. After sucessfull experiments with AUVs this industry became the first major commercial application of AUVs. Offshore hydrocarbon exploration is already well established: the number of offshore oil rigs is just below 500 and rising [6].

[1]The class organization of ROV, UUV and AUV may differ depending on the author. The adopted class organization is devised from DNV GL [1].

The mission of an AUV is dependent on its purpose. Although some mission scenarios are common for these vehicles, such as mapping and reconnaissance, it makes sense to organize characteristic applications in terms of purpose:

- **Military applications** - These range from intelligence, surveillance and reconnaissance to expeditionary and anti-submarine warfare and mine disposal. In *The Navy Unmanned Undersea Vehicle (UUV) Master Plan* [4] one can find more information about the US Navy's strategy to develop new and extend on current AUV capabilities.

- **Commercial applications** - Inspection, either for environmental or engineering purposes, of pipelines, communication lines and underwater structures are the primary commercial application of AUV's. [6, 7]. Other emerging applications include mapping and identification of underwater mineral deposits and inspection of aquaculture sites.

- **Research applications** - According to Wynn et al., 2014 [5] four main applications are devised that can be adapted to: habitat mapping in deep- and shallow-water; study of volcanic and hydrothermal vents; temperature monitoring; and mapping of ocean terrain.

These sectors are currently responsible for approximately 50%, 20% and 30%, respectively, of the AUV market (estimated 200 million (US$) in 2012). By contrast, the ROV market represented an estimated value of 850 million (US$) in the same period [2][2]. This discrepance can be credited to the high degree of maturaty of the ROV technology and limitations inherent to the nature of AUVs. Although autonomy, communications, navigation, data storage and short life cycles present complex challenges that limit the use of AUVs [3], these do not seem to compromise the use of AUVs for future missions since the AUV market is estimated to reach 2.3 billion (US$) by 2019 [2]. Furthermore, integration of marine technologies such as ROVs, AUVs, towed underwater vehicles and unmanned surface vehicles is an active field of research that may prove valuable.

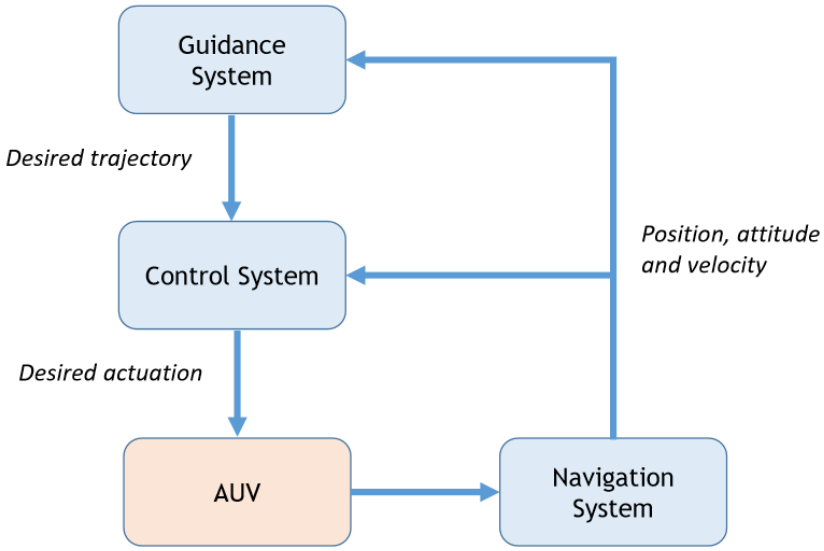

Figure 1.1: Guidance, navigation and control diagram.

[2]Source: Duke University Center on Globalization, Governance & Competitiveness (CGGC)

The autonomous nature of AUVs imply a high level of reboutness of the *guidance, navigation and control* system(s). One of the most challenging limitations for navigation is underwater communication: the high electrical conductivity of water inhibits the use of electromagnetic positioning (such as GPS[3]) and communication systems. The best available option is accustic systems, however, short range and low transfer rates restric its use for positioning and high data flux communication [3]. AUV navigation is therefore traditionally achieved by *inertial navigation systems* (INS) [8]. The data from the navigation system is relayed to the guidance system, this system is responsible for computing the desired motion that the vehicle should follow to achieve a given trajectory. A reference model is traditionally used to assure feasible trajectories. The control system can then determine the necessary forces and moments that should be imposed on the vehicle to achieve the desired motion. This forces and moments are imposed using the control actuators i.e. thrusters and control surfaces, if present [9].

1.1 Historical Overview of UUV's and Control Theory

The first vehicle that can be classified as an UUV is the Whitehead self-propelled torpedo, developed during the 1860's by Robert Whitehead [10, 11]. This vehicle can also be classified as the first AUV since it operated autonomously. Early torpedos operated using a Pendulum-and-hydrostat for depth-keeping and a gyroscopic steering system for course-keeping [11].

The early 20^{th} century marked the beginning and subsequent expansion of *feedback* controllers (see figure 1.2) for a number of applications, most notably, the PID (Proportional-Integral-Derivative) controller was first introduced on ships for automatic steering [12]. Although, simple control systems were being implemented, limitations of current methods and little understanding of the underlying mathematical principles in control meant that only so much could be achieved and most applications were based on a trial and error approach [13].

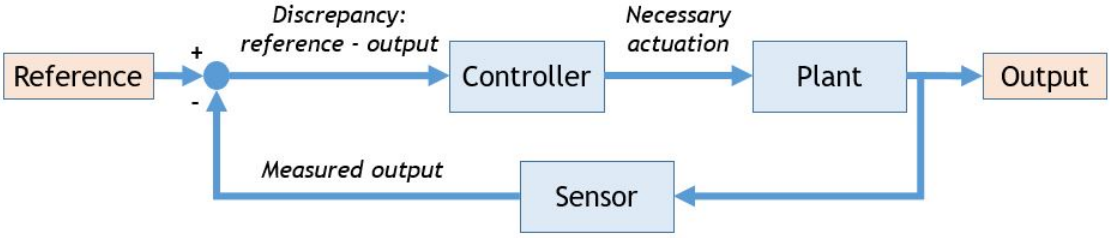

Figure 1.2: A block diagram of a negative feedback control system.

The development of unmanned submersibles remained limited to the torpedo until 1953 when the first ROV, nicknamed "poodle", was developed by Dimitri Rebikoff [14]. In control theory, the 1950's witnessed the advent of modern control: the popularization of the *state-space* approach, by engineers working in the aerospace industry, meant that complex physical models could be used for the design of feedback controllers. This new approach also facilitated the use of existing

[3]GPS: Global Positioning System.

tools of analysis for differential equations (e.g Lyapunov stability) and allowed for new concepts such as *observability* and *controllability* by Kalman [12, 13].

The initial development of AUV's started in the early 1960's and by the late 1960's, AUV's were used for military, research and oceanographic purposes. During the 1970's the discovery of oil in the North sea prompted the development of unmanned submersibles, mainly ROV's, capable of deep sea exploration and tasks associated with hydrocarbon exploration [6]. However, It was not until the 1980's and early 1990's that major leaps in computer technology allowed for small, powerful and reliable motion control. This technology allowed for a "boom" in AUV related research followed by routine commercial operations during the 2000's [15, 6, 16, 17, 18]. As the AUV technology matures, commercial and noncommercial markets are expected to grow [3].

1.2 Classification and Norms

AUV's are now classified as underwater robots (robot (as in *Encyclopaedia Britannica* [19]) - any automatically operated machine that replaces human effort, though it may not resemble human beings in appearance or perform functions in a human-like manner).

In *auvac.org* [20], a website dedicated to collect and share information about AUV systems, AUV's are differentiated in terms of purpose, body type and class. Up to twenty different purposes are devised for military applications, commercial use and scientific investigation. Eleven body types and four classes are discern. In *The Navy Unmanned Undersea Vehicle (UUV) Master Plan* [4] AUV's are organized by displacement and diameter. For the purpose of this thesis, displacement and body type are enough for classification.

1. Man-Portable class – Vehicle displacement from 10 kg to 50 kg.

2. Light Weight Vehicle class – Vehicle displacement of about 250 kg.

3. Heavy Weight Vehicle class – Vehicle displacement of about 1 400 kg.

4. Large Vehicle class – Vehicle displacement of about 10 000 kg.

This classification is far from proper and should be taken accordingly. However, it may serve as a precursor for a more significant classification.

A simple way to classify body types is by the number of hulls: single or multi. Most AUVs follow the single hull (or single body) configuration, with special emphasis on the torpedo shape. Probably the greatest advantage of such systems is in hydrodynamic efficiency due to ther lower contact area with the surrounding fluid. Multi-hull AUVs are typically comprised of two or three hulls. The Multi-hull configuration allows for greater flexibility in the distribution of of weight and buoyant force. Allocating heavy components to the lower body allows for the *center of buoyancy* (CB) to rise above the *center of gravity* (CG) by a considerable distance, thus assuring hydrostatic stability stability. Furthermore, the greater the distance between these centers,

refered to as the *metacentric height*, the more stable the vehicle. This could be significant when considering missions that require the vehicle to be as stable as possible e.g. mapping [21]. On the downside, drag forces and weight are typically greater for multiple body AUVs.

When designing a new product, the use of norms, ideally standards, in all stages of the project is of major importance. These help assure product feasibility. Although no standards exist for the control of AUVs, norms from *Det Norske Veritas Germanischer Lloyd* (DNV GL) are available [1]. The design of this AUV tries to comply with the norms from DNV GL.

1.3 The AUV

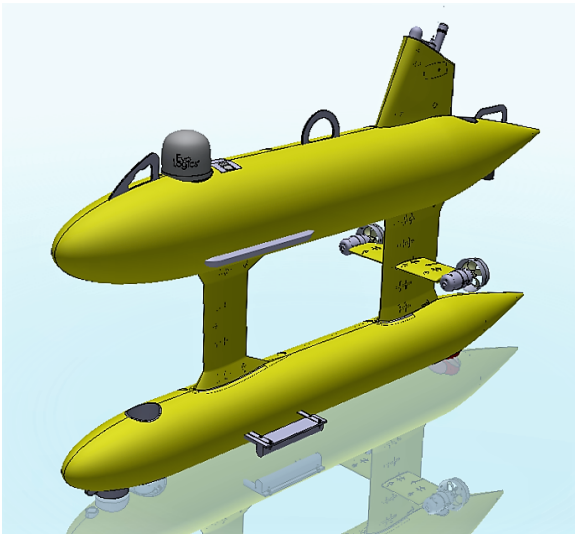

Figure 1.3: 3D model of the AUV being developed at CEiiA (courtesy of CEiiA).

The AUV being developed at CEiiA (see figure 1.3) is a double body, light weight research AUV capable of a Nominal Diving Depth (NDD)[4] of 3,000 meter.

The vehicle is comprised of two pressure hulls. The lower pressure hull houses the batteries and the upper one houses all necessary systems and sensors, as well as data storage equipment. The weight force is counteracted by adding low density syntactic foam which provides extra buoyancy. In order to increase the metacentric height, most syntactic foam is located in the upper body.

[4]Nominal Diving Depth - The maximum diving depth for unrestricted operation of an underwater vehicle (*In accordance with* [1]).

This AUV carries a variety of sensors for data acquisition and navigation. The sensors used for underwater navigation include:

- *Inertial Navigation System* (INS) - Comprised of *accelerometers* and *gyroscopes*. By integrating linear and angular accelerations this system allows estimation of position and velocity. The gyroscope determines the orientation.

- *Magnetometer* - Using electromagnets, the magnetometer determines the magnetic north by analyzing the disturbance in the electromagnet's magnetic field caused by the Earth's magnetic field.

- *Doppler Velocity Log* (DVL) - This equipment uses the acoustic Doppler principle to estimate velocity. It may or may not include ocean current estimation.

- *Underwater Altimeter* - The altitude is estimated by sending an acoustic signal towards the seabed. Knowing the velocity of sound in water it is possible to calculate the distance.

The propulsive system is comprised of four identical *thrusters*, two vertical and two horizontal. The vertical thrusters are embedded in the hulls: the forward engine in the lower body and the aft engine in the upper body. The position of the longitudinal thrusters can be seen in section 1.3. These provide the necessary force to propel the vehicle forward and, by applying a different force to each engine, allow the vehicle to change course.

An important feature of this vehicle is that the vertical and horizontal hydrodynamic fairings are designed to act as stabilizing surfaces. Considering that the vehicle is moving forward, the fairings induce lift forces that create a correcting moment. This is intended at keeping the vehicle parallel to the direction of the flow. The influence of the stabilizing surfaces in the general dynamics of the vehicle is addressed in section 3.2.5.

1.3.1 Mission

The AUV being developed at CEiiA follows the traditional research AUV mission, which can be divided into three main stages:

- *Dive* - Since ballast tanks are not present in this AUV, extra mass is carried in the bow to increase the weight force thus facilitating the descend. A spiral trajectory is to be performed through the water column with a nose down attitude (see figure 1.4). When mission depth is reached, this extra mass is released and residual buoyancy is achieved (see section 3.2.3).

- *Data acquisition* - The typical sensor suit of research AUVs requires the vehicle to be capable of stable longitudinal "flight" (small angles of attitude). The vehicle should be able of course keeping, changes in course and depth. A da aquisition scenario is performed using the lawn mower approach, in a similar manner than that of figure 1.5.

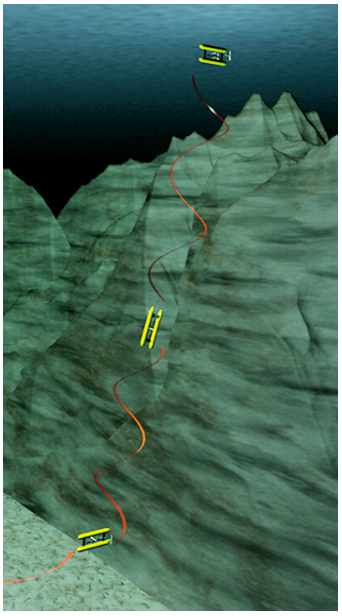

Figure 1.4: Diving and ascending scenario (courtesy of CEiiA).

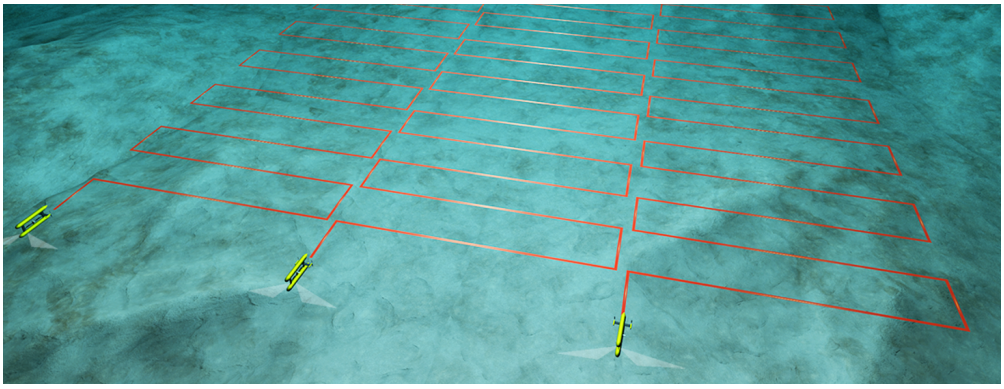

Figure 1.5: Mission scenario (courtesy of CEiiA).

- *Ascent* - Extra mass is also carried in the stern of the vehicle. When the mission is concluded the mass is released and buoyant forces overcome gravitational forces thus forcing the vehicle into a nose down ascent. Also to be preformed in a spiral manner (see figure 1.4).

1.3.2 Similar Vehicles

Although there are plenty of light weight AUVs, most are single body. Possibly the first successful double body, where both hulls are aligned vertically, AUV is the *SeaBed* thus, this configuration is sometimes referred as twin body type SeaBed.

- **Woods Hole Oceanographic Institution's SeaBed**

Figure 1.6: The Woods Hole Oceanographic Institution's SeaBed AUV (adapted from [22]).

The SeaBed platform (figure 1.6), available in various configurations, has participated in a number of research missions, being currently operated by multiple institutions around the world. The standard SeaBed platform has a mass of 250 kg, a length of 2.5 m, maximum diving depth of 2,000 m and an endurance of approximately 8 hours. The success of the SeaBed led to the development of the *Puma* and *Jaguar* which improved capabilities of their predecessor [22]. The SeaBed validated the concept of a twin, vertical aligned hull AUV.

- **Marport's SQX-500**

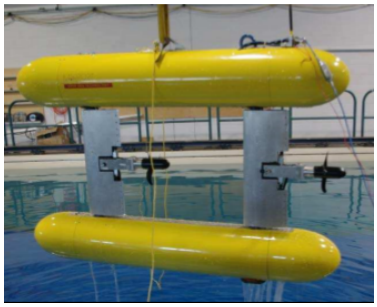

Figure 1.7: The Marport's SQX-500 UUV (adapted from [23]).

The Marport's SQX-500 is a more recent platform directed at military applications. The vehicle presents a mass of 95 kg, maximum diving depth of 500 meter, it is 1.6 meters long, has 8 hours of endurance and a cruise speed of 2 m/s. This vehicle is capable of moving its vertical rudders 180° in all directions, providing the SQX-500 with great maneuverability.

1.4 Terminology

"Nomenclature for Treating the Motion of a Submerged Body Through a Fluid" is the title of a 1950 report by the American *Society of Naval Architects and Marine Engineers* (SNAME) [24] that aimed to normalize nomenclature and notation in this field. This, or a similar version of it, is the most common nomenclature and notation used today when treating underwater vehicles, it is therefore used as reference for this thesis and will be address as SNAME notation hereinafter. Moreover, in recent years, Fossen's *Guidance and Control of Ocean Vehicles* [25] became a common reference for modeling purposes. In *Guidance and Control of Ocean Vehicles*, Fossen expands the SNAME notation to address certain particularities. Notation and arrangements in this reference are also adopted.

1.4.1 Motion

Underwater vehicles experience motion in 6 Degrees of Freedom (DoF), i.e. complete freedom of movement. Two categories can be devised when considering the nature of motion, 3DoF for translation and 3DoF for rotation. According to SNAME notation:

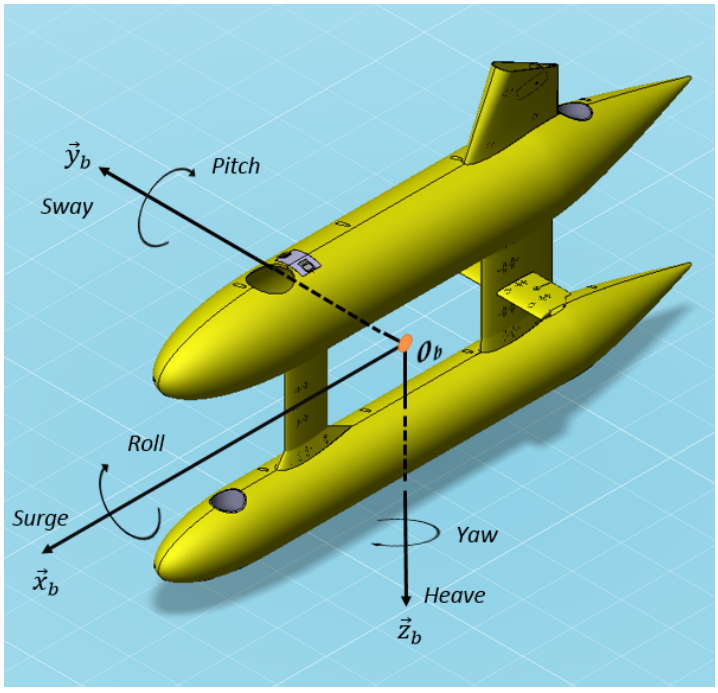

Figure 1.8: Motion variables for the body-fixed reference frame i.e.$\{b\} = (x_b, y_b, z_b)$
.

Table 1.1: Translation DoFs.

Terminology	Motion along	Position	Velocity	Force
Surge	x_b	x	u	X
Sway	y_b	y	v	Y
Heave	z_b	z	w	Z

Table 1.2: Rotational DoFs.

Terminology	Rotation about	Attitude	Angular velocity	Moment
Roll	x_b	ϕ	p	K
Pitch	y_b	θ	q	M
Yaw	z_b	ψ	r	N

Tables 1.1 and 1.2 presents terminology and notation for translation and rotation, respectively. Figure 1.8 summarizes motion for 6DoF.

1.4.2 Vector Notation for 6DoF

It is useful to express dynamic properties in vectorial notation for purposes of simplicity and organization. The adopted notation is now produced in the context of expressing motion in 6DoF. This includes organizing vectors by qualitative property and expressing them in terms of reference frames. Two types of reference frames are of interest for the purpose of this thesis: a *local North-East-Down* (NED) $\{n\}$ reference frame, which is inertial, and the *body-fixed* $\{b\}$ reference frame (see section 1.6.1.1).

Arrangement: The argument represents the physical property, the superscript represents the frame where this property is expressed, the subscript represents the point of action (if in fraction, the denominator denotes the reference point).

Example: $\boldsymbol{p}^e_{\frac{b}{n}}$ = Position of point 0_b (origin of $\{b\}$) with respect to $\{n\}$, expressed in $\{e\}$ reference frame.

- **Position vector** $\boldsymbol{p}^n_{\frac{b}{n}} = \begin{bmatrix} N \\ E \\ D \end{bmatrix} \in \mathbb{R}^3$

The position vector expresses the vehicle's position in 3D space in $\{n\}$ (see section 1.6.1.1).

- **Attitude vector**

$$\boldsymbol{\Theta}_{nb} = \begin{bmatrix} \phi \\ \theta \\ \psi \end{bmatrix} \in \mathbb{S}^3 \qquad \boldsymbol{q} = \begin{bmatrix} q_0 \\ q_1 \\ q_2 \\ q_3 \end{bmatrix} \in \mathbb{R}^4$$

- **Linear velocity vector** $\boldsymbol{v}^b_{\frac{b}{n}} = \begin{bmatrix} u \\ v \\ w \end{bmatrix} \in \mathbb{R}^3$

  Absolute velocity is given by the magnitude of the velocity vector (equation 1.3).

- **Angular velocity vector** $\boldsymbol{\omega}_{\frac{b}{n}}^{b} = \begin{bmatrix} p \\ q \\ r \end{bmatrix} \in \mathbb{R}^3$

- **Force vector** $\boldsymbol{f}_{b}^{b} = \begin{bmatrix} X \\ Y \\ Z \end{bmatrix} \in \mathbb{R}^3$

- **Moment vector** $\boldsymbol{m}_{b}^{b} = \begin{bmatrix} K \\ M \\ N \end{bmatrix} \in \mathbb{R}^3$

The complete vector representation for 6DoF can be expressed by the following vectors:

- **Position and attitude vector** $\boldsymbol{\eta} = \begin{bmatrix} \boldsymbol{p}_{\frac{b}{n}}^{n} \\ \boldsymbol{q} \end{bmatrix} \in \mathbb{R}^7 \quad ; \quad \boldsymbol{\eta} = \begin{bmatrix} \boldsymbol{p}_{\frac{b}{n}}^{n} \\ \boldsymbol{\Theta}_{nb} \end{bmatrix} \in \mathbb{R}^3 \times \mathbb{S}^3$

- **Velocity and acceleration vector** $\boldsymbol{\nu} = \begin{bmatrix} \boldsymbol{v}_{\frac{b}{n}}^{b} \\ \boldsymbol{\omega}_{\frac{b}{n}}^{b} \end{bmatrix} \in \mathbb{R}^6$

- **Force and moment vector** $\boldsymbol{\tau} = \begin{bmatrix} \boldsymbol{f}_{b}^{b} \\ \boldsymbol{m}_{b}^{b} \end{bmatrix} \in \mathbb{R}^6$

1.5 Overview of Dynamic Models for Underwater Vehicles

The post Second World War period saw the advent of the state-space approach. Simply put, the method involves modeling a system (or plant), such as an AUV, by creating a mathematical model which is represented by first-order differential equations. The controller is design to satisfy model particularities. In the context of this thesis, the dynamic model is the set of first order differential equations that describe the vehicle's motion. Simulation of the dynamic model is achieved by solving this equations by integration [26].

The standard equations of motion for submarines were published in 1967 by Gertler, at the request of the US Navy and can be found in [27]. These equations were subsequently revised in 1979 by Feldman [28]. The standard equations of motion for submarines are highly accurate due to the extent to which the hydrodynamic coefficients are addressed [29]. The intrinsic nature of manned submarines introduces the need for such accurate models and the state-of-art in hydrodynamic modeling, most notably in terms of test facilities and man-power. The costs associated with the development of AUVs do not compare to those of a manned submarine

[30]. On the other hand, unlike submarines, AUVs operate autonomously so robust and accurate control is paramount. In this context, it is of the utmost importance to evaluate requirements and capacity in order to choose the appropriate modeling approach.

Some of the most important considerations are summarized below:

- The mission (discussed in section 1.3) does not require extreme maneuvering capability.
- High speed is not required.
- No experimental tests are possible at the time.
- Since control is the main purpose, applicability of modern control methods is important.

In the context of these considerations it is clear that the standard equations of motion for submarines are not the answer since very detailed hydrodynamic characterization is not possible. However, other, less complex options are available. In *Modeling and simulation of the autonomous underwater vehicle, Autolycus* [30], Tang compares the most popular ethods for modeling AUVs: Humphrey's, Nahon's and Fossen's models.

- Humphrey's model - Humphrey [31] used symmetry and other simplifications to linearize the equations of motion and decouple the longitudinal and lateral motion. The transfer functions are also provided for simpler implementation. However, no methods are provided to estimate hydrodynamic coefficients.
- Nahon's model - This model follows a different approach to that of Humphrey's. Instead of linearizing the model, Nahon searched for methods to estimate coefficients solely by the vehicle's geometry, using both computational and analytical methods for the effect, while retaining the nonlinear nature of the equations of motion [32].
- Fossen's model - Undoubtedly the most used method in modern literature, this model shares characteristics with the latter, the great advantage is that the equations of motion are arranged to facilitate the use o nonlinear control tools [29]. The model is a set of nonlinear equations arranged in matrix form and simple methods to estimate hydrodynamic coefficients are provided to a certain extent [33].

Since it is a proven method and satisfies the considerations discussed in this section, Fossen's model is used for modeling the AUV being developed at CEiiA. Fossen's model can be expressed in accordance with Fossen's *Nonlinear Modelling and Control of Underwater Vehicles* [33].

$$\dot{\boldsymbol{\eta}} = \boldsymbol{J}(\boldsymbol{\eta})\boldsymbol{\nu} \quad (1.1)$$

$$\boldsymbol{M}\dot{\boldsymbol{\nu}} + \boldsymbol{C}(\boldsymbol{\nu})\boldsymbol{\nu} + \boldsymbol{D}(\boldsymbol{\nu})\boldsymbol{\nu} + \boldsymbol{g}(\boldsymbol{\eta}) = \boldsymbol{\tau} \quad (1.2)$$

Equation 1.1 represents *kinematics* and equation 1.2 represents *kinetics* (see section 1.6). Where $\boldsymbol{J}$ is a vector transformation matrix. $\boldsymbol{M}$, $\boldsymbol{C}$ and $\boldsymbol{D}$ denote the mass, Coriolis and Damping, respectively, $\boldsymbol{g}(\boldsymbol{\eta})$ represents the hydrostatic forces and $\boldsymbol{\tau}$ is the applied external forces vector.

1.6 Fossen's Model for Marine Craft

Dynamics can be divided into two branches of classic mechanics: kinematics and kinetics.

The geometric aspects of motion are addressed in kinematics. This includes attitude, position, velocity, acceleration and subsequent concepts such as trajectory, rotation, reference frames, etc. In turn, kinetics is the study of internal and external forces and moments that dictate the dynamic characteristics of a given vehicle.

1.6.1 Kinematics

This section addresses the different aspects of kinematics. A brief description of the used reference frames in the context of *Galilean relativity* is produced. Navigation angles are subsequently presented and the problematic of vector transformation between reference frames is also addressed.

1.6.1.1 Reference Frames

Understanding reference frames is essential when modeling vehicles considering that our main concern is motion, and motion is relative to some reference. For navigation in large areas, the earth-centered, earth-fixed (ECEF) reference frame $\{e\} = (x_e, y_e, z_e)$ is used, yet, considering that the vehicle is moving at low speed and operating in an area where variations in latitude

and longitude are small, a local reference frame can be adopted. In this context, two reference frames are selected to express and simulate motion. The body-fixed and a local NED reference frames [9]. These Cartesian frames follow the *right hand rule*.

- **Local NED** $\{n\} = (x_n, y_n, z_n)$ - An inertial reference frame that represents a tangent plane normal to a fixed point 0_n (the reference frame's origin), in the earth's surface. The $\{n\}$ vector components are respective representations of north, east and down coordinates.

- **Body-fixed** $\{b\} = (x_b, y_b, z_b)$ - A non-inertial reference frame that is coupled to the body. This frame exhibits rotation and acceleration relative to the Earth-fixed inertial reference frame. The $\{b\}$ vector components represent, respectively, the longitudinal, transverse and normal axes of the vehicle (see figure 1.8). The origin is expressed as 0_b.

Considerations of the Body-fixed reference frame The center of the Body-fixed reference frame $\{b\}$ is usually appointed, either to coincide with the center of gravity (CG) or in some geometrically meaningful location, since this locations are typically well defined and less likely to suffer modification e.g. location symmetry planes intersection, geometrical midpoints, etc.

Two important point to consider when designing an underwater vehicle are the CG and the CB.

$\mathbf{r}_g^b = \begin{bmatrix} x_g & y_g & z_g \end{bmatrix}^T$ denotes the position vector for CG with respect to 0_b.

$\mathbf{r}_B^b = \begin{bmatrix} x_B & y_B & z_B \end{bmatrix}^T$ denotes the position vector for CB with respect to 0_b.

1.6.1.2 Navigation angles

Flow related angles When a vehicle travels through a fluid, the incidence of the flow relative to the body axes i.e. the velocity vector is of great importance because the hydrodynamic forces are perpendicular (drag) and parallel (lift) to the flow. This suggests that another, "flow oriented", reference frame can be devised. This frame is commonly referred as *flow axes* ($\{f\} = (x_f, y_f, z_f)$). The origin of $\{s\}$ frame is the same as the $\{b\}$ frame.

The angle between x_b and the projection of x_f in the $x_b z_b$ plane is denoted *angle of attack* (AoA or α).

The angle between x_b and the projection of x_f in the $x_b y_b$ plane is denoted *side-slip angle* (β).

Although flow axes can be useful for hydrodynamic analysis, a perhaps simpler way to determine the angle of attack and the side-slip angle is by analyzing the velocity vector $\boldsymbol{v}_{\frac{b}{n}}^{b}$. The magnitude of the velocity vector is expressed by:

$$U = \sqrt{u^2 + v^2 + w^2} \quad (1.3)$$

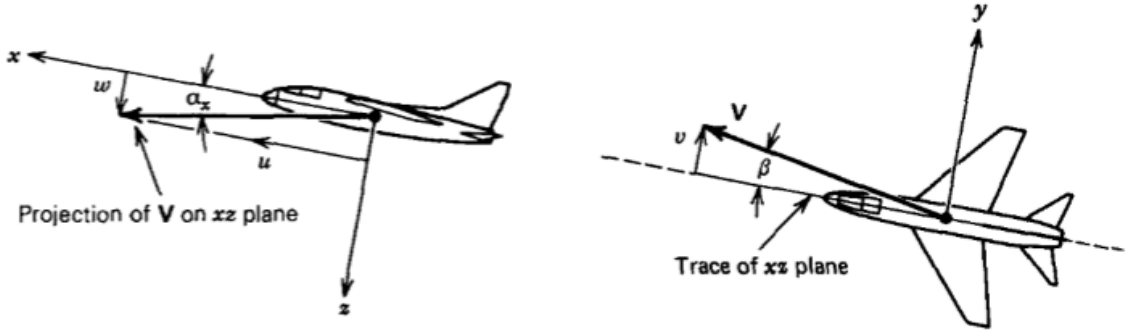

Figure 1.9: Definition of angle of attack and side-slip, respectively (adapted from [34]).

From figure 1.9,and in accordance with [34], the following relation between velocity and these angles can be devised.

$$\alpha = \tan^{-1}(\frac{w}{u}) \quad (1.4)$$
$$\beta = \sin^{-1}(\frac{v}{U}) \quad (1.5)$$

Orientation related angles When navigating, whether for aircraft or marine craft, north is used as the orientation of reference, expressed in compasses as zero degrees. Following the NED Cartesian system and right hand rule, 90° points towards East, 180° towards South and 270° towards West. The angle between the projection of x_b in the $x_b y_b$ plane and x_n defines *heading* (ϕ). If a side-slip angle is present, heading is not the direction of travel, the direction of travel is then denominated *course* (χ) and it is defined as the the sum of the side-slip angle and heading angle:

$$\chi = \beta + \phi. \quad (1.6)$$

1.6.1.3 Transformation between Reference Frames

The underlying problem in transforming vectors between reference frames whose axes are not aligned is rotation. A handful of methods can be used to achieve vector rotation, but the two

most common methods are Euler angles and quaternions. Transformation using quaternions is significantly faster, in terms of computation, and singularities are avoid. However, Euler angles are more intuitive [35],[36], [37],[38]. Both quaternions and Euler angles were used for the 6DoF model (see chapter 4). For the purpose of data presentation and to devise the longitudinal and lateral subsystems (see chapter 2), Euler angles were used.

Quaternion Quaternions are a 4th order complex number system introduced by William R. Hamilton in 1843 and present similar properties to complex numbers. When considering the imaginary and real parts of a complex number as coordinate axis of the Cartesian plane, an association can be devised and used to translate and rotate a point and hence to transform a vector. However, for a 3D geometry, 4th order complex numbers are necessary to obtain similar capacities [39].

A quaternion q can be expressed as:

$$q = q_o + q_1 i + q_2 j + q_3 k \quad (1.7)$$

Note that:

$$i^2 = j^2 = k^2 = ijk = -1$$

Expressed in vector form:

$$\mathbf{q} = \begin{bmatrix} q_0 & \boldsymbol{\varepsilon} \end{bmatrix}^T \in \mathbb{R}$$

Where,

$$\boldsymbol{\varepsilon} = \begin{bmatrix} q_1 \\ q_2 \\ q_3 \end{bmatrix} \in \mathbb{R}^{\nVdash}$$

1.6.1.4 Linear Velocity Transformation

Transformation is attained by means of multiplying the body's velocity vector by a *rotation matrix* $\mathbf{R}_{to}^{from}$.

For quaternions linear velocity transformation can be expressed like:

$$\dot{\mathbf{p}}_{b/n}^{n} = \mathbf{R}_{b}^{n}(\mathbf{q})\boldsymbol{\upsilon}_{b/n}^{b} \quad (1.8)$$

Where:

$$\mathbf{R}_b^n(\mathbf{q}) = \begin{bmatrix} 1-2(q_2^2+q_3^2) & 2(q_1q_2-q_3q_0) & 2(q_1q_3+q_2q_0) \\ 2(q_1q_2+q_3q_0) & 1-2(q_1^2+q_3^2) & 2(q_2q_3+q_1q_0) \\ 2(q_1q_3+q_2q_0) & 2(q_2q_3+q_1q_0) & 1-2(q_1^2+q_2^2) \end{bmatrix}$$

And for Euler angles:

$$\dot{\mathbf{p}}_{b/n}^n = \mathbf{R}_b^n(\boldsymbol{\Theta}_{\boldsymbol{nb}})\boldsymbol{\upsilon}_{b/n}^b \quad (1.9)$$

Where:

$$\mathbf{R}_b^n(\boldsymbol{\Theta}_{\boldsymbol{nb}}) = \begin{bmatrix} \cos(\psi)\cos(\theta) & -\sin(\psi)\cos(\phi)+\cos(\psi)\sin(\theta)\sin(\phi) & \sin(\psi)\sin(\phi)+\cos(\psi)\sin(\theta)\cos(\phi) \\ \sin(\psi)\cos(\theta) & \cos(\psi)\cos(\theta)+\sin(\phi)\sin(\theta)\sin(\psi) & -\cos(\psi)\sin(\phi)+\sin(\theta)\sin(\psi)\cos(\theta) \\ -\sin(\theta) & \cos(\theta)\sin(\phi) & \cos(\theta)\cos(\phi) \end{bmatrix}$$

Note that $(\mathbf{R}_b^n)^{-1} = (\mathbf{R}_b^n)^T$.

Angular Velocity Transformation Transformation is attained by means of multiplying the vector of interest by a *transformation matrix* $\mathbf{T}$.

For quaternions:

$$\dot{\mathbf{q}} = \mathbf{T}_q(\mathbf{q})\boldsymbol{\omega}_{b/n}^b \quad (1.10)$$

Where:

$$\mathbf{T}_q(\mathbf{q}) = \begin{bmatrix} -q_1 & -q_2 & -q_3 \\ q_0 & -q_3 & q_2 \\ q_3 & q_0 & -q_1 \\ -q_2 & q_1 & q_0 \end{bmatrix}$$

For Euler angles:

$$\dot{\boldsymbol{\Theta}}_{\boldsymbol{nb}} = \mathbf{T}_\Theta(\boldsymbol{\Theta}_{\boldsymbol{nb}})\boldsymbol{\omega}_{b/n}^b \quad (1.11)$$

Where:

$$\mathbf{T}_{\Theta}(\boldsymbol{\Theta_{nb}}) = \begin{bmatrix} 1 & \sin(\phi)\tan(\theta) & \cos(\phi)\tan(\theta) \\ 0 & \cos(\phi) & -\sin(\phi) \\ 0 & \sin(\phi)/\cos(\theta) & \cos(\phi)/\cos(\theta) \end{bmatrix}$$

1.6.1.5 Kinematics Equation

Since $\boldsymbol{\eta} = \begin{bmatrix} \boldsymbol{p}^n_{\frac{b}{n}} \\ \boldsymbol{q} \end{bmatrix}$, the kinematics equation for an AUV moving in the $\{n\}$ reference frame is expressed as:

$$\dot{\boldsymbol{\eta}} = \boldsymbol{J}(\boldsymbol{\eta})\boldsymbol{\nu} \quad (1.12)$$

- If using quaternions:

$$\dot{\boldsymbol{\eta}} = \boldsymbol{J}_q(\boldsymbol{\eta})\boldsymbol{\nu} \quad (1.13)$$

Equation 1.13 expands to:

$$\begin{bmatrix} \dot{\boldsymbol{p}}^n_{\frac{b}{n}} \\ \dot{\boldsymbol{q}} \end{bmatrix} = \begin{bmatrix} \mathbf{R}^n_b(\boldsymbol{q}) & \mathbf{0}_{3\times3} \\ \mathbf{0}_{3\times3} & \mathbf{T}(\boldsymbol{q}) \end{bmatrix} \cdot \begin{bmatrix} \boldsymbol{v}^b_{\frac{b}{n}} \\ \boldsymbol{\omega}^b_{\frac{b}{n}} \end{bmatrix}$$

- If using Euler angles:

$$\dot{\boldsymbol{\eta}} = \boldsymbol{J}_{\Theta}(\boldsymbol{\eta})\boldsymbol{\nu} \quad (1.14)$$

Equation 1.14 expands to:

$$\begin{bmatrix} \dot{\boldsymbol{p}}^n_{\frac{b}{n}} \\ \dot{\boldsymbol{\Theta}}_{\boldsymbol{nb}} \end{bmatrix} = \begin{bmatrix} \mathbf{R}^n_b(\boldsymbol{\Theta_{nb}}) & \mathbf{0}_{3\times3} \\ \mathbf{0}_{3\times3} & \mathbf{T}(\boldsymbol{\Theta}_{nb}) \end{bmatrix} \cdot \begin{bmatrix} \boldsymbol{v}^b_{\frac{b}{n}} \\ \boldsymbol{\omega}^b_{\frac{b}{n}} \end{bmatrix}$$

1.6.2 Kinetics

Kinetics, as previously stated, addresses the relationship between motion and force. An underwater vehicle is exposed to the same laws of motion that govern all bodies, under the assumption that the vehicle can be considered rigid, these laws are traditionally referred to as the equations of motion for a rigid body. Since the surrounding fluid is water, a variety of hydrostatic and hydrodynamic forces are also present. The influence of these forces is mostly dependent on the geometry and mass of the vehicle. Estimation of parameters of interest presents a complex task which is addressed in chapter 3. For the purpose of this thesis, three assumptions are devised from an early stage in the project:

- *Low operational velocities.*
- *Ocean currents are unaccounted for.*
- *Operating area is large enough for unrestricted motion.*

Other vehicle-specific constrains are expressed in section 3.2.1.

1.6.2.1 Rigid-Body Equations of motion

The relationship between motion and force in the context of *classical mechanics* was introduced by Isaac Newton in *Philosophiæ Naturalis Principia Mathematica* Newton's Three Laws of Motion [40]. Considering the vehicle is rigid, the 6DoF rigid-body equations of motion can be expressed, in matrix form, as:

$$\boldsymbol{M}_{rb} \cdot \dot{\boldsymbol{\nu}} + \boldsymbol{C}_{rb}(\boldsymbol{\nu}) \cdot \boldsymbol{\nu} \quad (1.15)$$

Where $\boldsymbol{M}_{rb}$ is the rigid body mass matrix and $\boldsymbol{C}_{rb}$ represents the rigid body Coriolis forces matrix. The rigid body mass matrix is expressed according to Fossen, 2011 [9]:

$$\boldsymbol{M}_{rb} = \begin{bmatrix} m \cdot \mathbf{I}_{3\times 3} & -\mathbf{S}(\mathbf{r}_g^b) \\ m \cdot \mathbf{S}(\mathbf{r}_g^b) & \mathbf{I}_b \end{bmatrix} \quad (1.16)$$

Where m is the mass of the vehicle, $\mathbf{I}_{3\times3}$ is a 3×3 identity matrix, $\mathbf{S}(\mathbf{r}_g^b)$ is the skew-symmetric matrix[5] of $\mathbf{r}_g^b$ and $\mathbf{I}_b$ is the vehicle's inertia tensor. This expands to:

$$\boldsymbol{M}_{rb} = \begin{bmatrix} m & 0 & 0 & 0 & m\cdot z_g & -m\cdot y_g \\ 0 & m & 0 & -m\cdot z_g & 0 & m\cdot x_g \\ 0 & 0 & m & m\cdot y_g & -m\cdot x_g & 0 \\ 0 & -m\cdot z_g & m\cdot y_g & I_x & -I_{xy} & -I_{xz} \\ m\cdot z_g & 0 & -m\cdot x_g & -I_{yx} & I_y & -I_{yz} \\ -m\cdot y_g & m\cdot x_g & 0 & -I_{zx} & -I_{zy} & I_z \end{bmatrix} \tag{1.17}$$

When an object's movement is expressed in terms of a non inertial reference frame, in this case the Body-fixed reference frame, additional forces seem to appear, the *Coriolis* and centrifugal forces [9].

The Coriolis and centrifugal forces matrix can be expressed according to Fossen and Fjellstad, 2005 [35].

$$\boldsymbol{C}_{rb}(\boldsymbol{\nu}) = \begin{bmatrix} \mathbf{0}_{3\times3} & -m\cdot\mathbf{S}(\boldsymbol{\nu}_1) - m\cdot\mathbf{S}(\boldsymbol{\nu}_2)\cdot\mathbf{S}(\mathbf{r}_g^b) \\ -m\cdot\mathbf{S}(\boldsymbol{\nu}_1) + m\cdot\mathbf{S}(\mathbf{r}_g^b)\cdot\mathbf{S}(\boldsymbol{\nu}_2) & -\mathbf{S}(\mathbf{I}_b\boldsymbol{\nu}_2) \end{bmatrix} \tag{1.18}$$

$$= \begin{bmatrix} 0 & 0 & 0 & m(y_gq+z_gr) & -m(x_gq-w) & -m(x_gr+v) \\ 0 & 0 & 0 & -m(y_gp+w) & m(z_gr+x_gp) & -m(y_gr-u) \\ 0 & 0 & 0 & -m(z_gp-v) & -m(z_gq+u) & m(x_gp+y_gq) \\ -m(y_gq+z_gr) & m(y_gp+w) & m(z_gp-v) & 0 & -I_{yz}q-I_{xz}p+I_zr & I_{yz}r+I_{xy}p-I_yq \\ m(x_gq-w) & -m(z_gr+x_gp) & m(z_gq+u) & I_{yz}q+I_{xz}p-I_zr & 0 & -I_{xz}r-I_{xy}q+I_xp \\ m(x_gr+v) & m(y_gr-u) & -m(x_gp+y_gq) & -I_{yz}r-I_{xy}p+I_yq & I_{xz}r+I_{xy}q-I_xp & 0 \end{bmatrix}$$

Proof of $\boldsymbol{C}_{rb}$ and $\boldsymbol{M}_{rb}$ can be found in [33].

[5] A matrix $\boldsymbol{A}$ is said to be skew-symmetric if $\boldsymbol{A}^T = -\boldsymbol{A}$

1.6.2.2 Hydrostatics

In hydrostatics, two forces are considered: *buoyancy* and *gravitational forces*.

Archimedes' principle - A body immersed in a fluid is subjected to an upwards force equal to the weight of the displaced fluid [41]. This force is designated as buoyancy force.

$$B = \rho g \nabla \quad (1.19)$$

Where ρ is the density of the fluid, g is the acceleration of gravity and ∇ is the volume of fluid displaced by the vehicle. The buoyancy force acts upon CB, parallel to z_n, in the negative direction. Expressed in $\{n\}$:

$$\boldsymbol{f}_B^n = \begin{bmatrix} 0 \\ 0 \\ -B \end{bmatrix} \quad (1.20)$$

The gravitational force (or weight) is derived from Newton's 2nd Law of motion.

$$W = mg \quad (1.21)$$

Where m is the mass and g is the acceleration of gravity. The gravitational force acts upon the CG, parallel to z_n, in the positive direction. Expressed in $\{n\}$:

$$\boldsymbol{f}_g^n = \begin{bmatrix} 0 \\ 0 \\ W \end{bmatrix} \quad (1.22)$$

Expressed in $\{b\}$:

$$\boldsymbol{f}_B^b = \mathbf{R}_b^n(q)^{-1} \boldsymbol{f}_B^n \quad (1.23)$$

$$\boldsymbol{f}_g^b = \mathbf{R}_b^n(q)^{-1} \boldsymbol{f}_g^n \quad (1.24)$$

The resulting forces and moments are referred to as *restoring forces*. The restoring forces vector $\boldsymbol{g}(\boldsymbol{\eta})$ can be expressed as:

$$\boldsymbol{g}(\boldsymbol{\eta}) = -\begin{bmatrix} \boldsymbol{f}_B^b + \boldsymbol{f}_g^b \\ \mathbf{r}_B^b \boldsymbol{f}_B^b + \mathbf{r}_g^b \boldsymbol{f}_g^b \end{bmatrix} \quad (1.25)$$

If using Euler angles, this expands to:

$$\boldsymbol{g}(\boldsymbol{\eta}) = \begin{bmatrix} (W-B)\sin(\theta) \\ -(W-B)\cos(\theta)\sin(\phi) \\ -(W-B)\cos(\theta)\cos(\phi) \\ -(y_g W - y_B B)\cos(\theta)\cos(\phi) + (z_g W - z_B B)\cos(\theta)\sin(\phi) \\ (z_g W - z_B B)\sin(\theta) + (x_g W - x_B B)\cos(\theta)\cos(\phi) \\ -(x_g W - x_B B)\cos(\theta)\sin(\phi) - (y_g W - y_B B)\sin(\theta) \end{bmatrix} \quad (1.26)$$

1.6.2.3 Hydrodynamic Added Mass

When a vehicle accelerates through a fluid a phenomena occurs in which some of the vehicles kinetic energy is transferred to the fluid due to friction, this results in extra resistance to accelerations. If the fluid density is much lower than the vehicle's e.g. air, this effect can be neglected yet, if those are similar, the vehicle behaves as if it had more mass then it actually does. Hence, the phenomena is generally known as *added mass*. If the mean is water, one can address this phenomena as *hydrodynamic added mass*.

In [42], the complete expressions for added mass are produced for an ideal fluid.

The kinetic energy of the fluid surrounding the vehicle $\boldsymbol{T}_A$ can be expressed according to [42]:

$$T_A = \frac{1}{2}\boldsymbol{\nu}\boldsymbol{M}_A\boldsymbol{\nu}^T \quad (1.27)$$

Where $\boldsymbol{M}_A$ is the added mass matrix:

$$\boldsymbol{M}_A = -\begin{bmatrix} X_{\dot{u}} & X_{\dot{v}} & X_{\dot{w}} & X_{\dot{p}} & X_{\dot{q}} & X_{\dot{r}} \\ Y_{\dot{u}} & Y_{\dot{v}} & Y_{\dot{w}} & Y_{\dot{p}} & Y_{\dot{q}} & Y_{\dot{r}} \\ Z_{\dot{u}} & Z_{\dot{v}} & Z_{\dot{w}} & Z_{\dot{p}} & Z_{\dot{q}} & Z_{\dot{r}} \\ K_{\dot{u}} & K_{\dot{v}} & K_{\dot{w}} & K_{\dot{p}} & K_{\dot{q}} & K_{\dot{r}} \\ M_{\dot{u}} & M_{\dot{v}} & M_{\dot{w}} & M_{\dot{p}} & M_{\dot{q}} & M_{\dot{r}} \\ N_{\dot{u}} & N_{\dot{v}} & N_{\dot{w}} & N_{\dot{p}} & N_{\dot{q}} & N_{\dot{r}} \end{bmatrix} \tag{1.28}$$

As defined by SNAME [24], the upper half of the matrix elements represents the typical inertia coefficient i.e. the derivative of the force component with respect to an acceleration (linear or angular) component, e.g. $X_{\dot{u}} = \frac{\partial X}{\partial \dot{u}}$. The lower half of the matrix elements represents the typical moment of inertia coefficient i.e. the derivative of the moment component with respect to a acceleration component, e.g. $K_{\dot{u}} = \frac{\partial K}{\partial \dot{u}}$.

Alternatively, this can be understood as the corresponding axial force or moment due to an acceleration.

Experimental methods are typicaly used to estimate hydrodynamic coeficients, however, analytical methods are also used to estimate added mass, either by specialized programs, like *WAMIT* [6] or *ESAM* [43], or by simplifying the vehicle's shape so that complex, time-consuming expressions can be avoided. Recently though, transient analysis in CFD has produced results in accordance with theoretical ones [44].

The Coriolis matrix due to added mass is expressed as:

$$\boldsymbol{C}_A(\boldsymbol{\nu}) = \begin{bmatrix} 0 & 0 & 0 & 0 & -a_3 & a_2 \\ 0 & 0 & 0 & a_3 & 0 & -a_1 \\ 0 & 0 & 0 & -a_2 & a_1 & 0 \\ 0 & -a_3 & a_2 & 0 & -b_3 & b_2 \\ a_3 & 0 & -a_1 & b_3 & 0 & -b_1 \\ -a_2 & a_1 & 0 & -b_2 & b_1 & 0 \end{bmatrix} \tag{1.29}$$

[6] http://www.wamit.com/

Where,

$$
\begin{aligned}
a_1 &= X_{\dot{u}}u + X_{\dot{v}}v + X_{\dot{w}}w + X_{\dot{p}}p + X_{\dot{q}}q + X_{\dot{r}}r \\
a_2 &= Y_{\dot{u}}u + Y_{\dot{v}}v + Y_{\dot{w}}w + Y_{\dot{p}}p + Y_{\dot{q}}q + Y_{\dot{r}}r \\
a_3 &= Z_{\dot{u}}u + Z_{\dot{v}}v + Z_{\dot{w}}w + Z_{\dot{p}}p + Z_{\dot{q}}q + Z_{\dot{r}}r \\
b_1 &= K_{\dot{u}}u + K_{\dot{v}}v + K_{\dot{w}}w + K_{\dot{p}}p + K_{\dot{q}}q + K_{\dot{r}}r \\
b_2 &= M_{\dot{u}}u + M_{\dot{v}}v + M_{\dot{w}}w + M_{\dot{p}}p + M_{\dot{q}}q + M_{\dot{r}}r \\
b_3 &= N_{\dot{u}}u + N_{\dot{v}}v + N_{\dot{w}}w + N_{\dot{p}}p + N_{\dot{q}}q + N_{\dot{r}}r
\end{aligned}
$$

1.6.2.4 Hydrodynamic Damping

Since the density of water is high when compared to other means where earth vehicles operate, drag forces are greater. Even at low speeds, like the ones experienced by most UUV, the drag component is considerable and should therefore be modeled correctly. More over, due to high fluid viscosity, this property should be taken into account.

The drag force can be modeled using the *drag equation*:

$$F_D = -\frac{1}{2}\rho\, C_D\, A_0 V^2 \quad \text{(1.30)}$$

Where C_D is the is the drag coefficient, A_0 represents the reference area and V is the velocity. 6DoF Damping for underwater vehicles can be described mathematically as:

$$
\boldsymbol{D}_n(\boldsymbol{\nu})\boldsymbol{\nu} = \begin{bmatrix}
|\,\boldsymbol{\nu}\,|^T\, \boldsymbol{D}_{n1}\boldsymbol{\nu} \\
|\,\boldsymbol{\nu}\,|^T\, \boldsymbol{D}_{n2}\boldsymbol{\nu} \\
|\,\boldsymbol{\nu}\,|^T\, \boldsymbol{D}_{n3}\boldsymbol{\nu} \\
|\,\boldsymbol{\nu}\,|^T\, \boldsymbol{D}_{n4}\boldsymbol{\nu} \\
|\,\boldsymbol{\nu}\,|^T\, \boldsymbol{D}_{n5}\boldsymbol{\nu} \\
|\,\boldsymbol{\nu}\,|^T\, \boldsymbol{D}_{n6}\boldsymbol{\nu}
\end{bmatrix} \quad \text{(1.31)}
$$

Where $\boldsymbol{D}_{ni}$, $i = 1, 2, ..., 6$, are 6×6 matrices.

The hydrodynamic damping i.e. drag, of an underwater vehicle can be highly coupled and nonlinear. If moving with low velocity, it is common to use quadratic approximation:

$$\boldsymbol{D}(\boldsymbol{\nu}) = \boldsymbol{D}_l + \boldsymbol{D}_q(\boldsymbol{\nu}) \quad (1.32)$$

Where:

$$\boldsymbol{D}_l = - \begin{bmatrix} X_u & X_v & X_w & X_p & X_q & X_r \\ Y_u & Y_v & Y_w & Y_p & Y_q & Y_r \\ Z_u & Z_v & Z_w & Z_p & Z_q & Z_r \\ K_u & K_v & K_w & K_p & K_q & K_r \\ M_u & M_v & M_w & M_p & M_q & M_r \\ N_u & N_v & N_w & N_p & N_q & N_r \end{bmatrix} \quad (1.33)$$

$$\boldsymbol{D}_q(\boldsymbol{\nu}) = - \begin{bmatrix} X_{u|u|} \mid u \mid & X_{v|v|} \mid v \mid & X_{w|w|} \mid w \mid & X_{p|p|} \mid p \mid & X_{q|q|} \mid q \mid & X_{r|r|} \mid r \mid \\ Y_{u|u|} \mid u \mid & Y_{v|v|} \mid v \mid & Y_{w|w|} \mid w \mid & Y_{p|p|} \mid p \mid & Y_{q|q|} \mid q \mid & Y_{r|r|} \mid r \mid \\ Z_{u|u|} \mid u \mid & Z_{v|v|} \mid v \mid & Z_{w|w|} \mid w \mid & Z_{p|p|} \mid p \mid & Z_{q|q|} \mid q \mid & Z_{r|r|} \mid r \mid \\ K_{u|u|} \mid u \mid & K_{v|v|} \mid v \mid & K_{w|w|} \mid w \mid & K_{p|p|} \mid p \mid & K_{q|q|} \mid q \mid & K_{r|r|} \mid r \mid \\ M_{u|u|} \mid u \mid & M_{v|v|} \mid v \mid & M_{w|w|} \mid w \mid & M_{p|p|} \mid p \mid & M_{q|q|} \mid q \mid & M_{r|r|} \mid r \mid \\ N_{u|u|} \mid u \mid & N_{v|v|} \mid v \mid & N_{w|w|} \mid w \mid & N_{p|p|} \mid p \mid & N_{q|q|} \mid q \mid & N_{r|r|} \mid r \mid \end{bmatrix} \quad (1.34)$$

As defined by [24], the upper half elements represent the typical static force derivative and the lower half represent the typical static moment derivative.

Drag forces are traditionally modeled using experimental methods. Analytical methods are too complex, except for simple shapes [45]. Alternatively, computational methods can and have been exploited to some extent (see references [46, 47]).

1.6.2.5 External Forces

The force that moves an AUV is typically provided by trolling motors. The external forces vector τ (or thrust vector) relates the geometric and thrust characteristics of each motor with the resultant forces and moments.

For vehicles controled by thrusters, the thrust vector can be expresses as in [48]:

$$\boldsymbol{\tau} = \boldsymbol{L}\boldsymbol{U} \quad (1.35)$$

Where $\boldsymbol{U}$ is the force vector representing the thrust provided by each motor and $\boldsymbol{L}$ is the mapping matrix that relates motor thrust to resulting forces and moments. An example of a mapping matrix can also be found in [48].

1.7 Complete Dynamic Model

The complete dynamic model is the association of the kinematic and kinetic equations (equations 1.1 and 1.2, repectively).

$$\begin{aligned} \dot{\boldsymbol{\eta}} &= \boldsymbol{J}(\boldsymbol{\eta})\boldsymbol{\nu} \\ \boldsymbol{M}\dot{\boldsymbol{\nu}} + \boldsymbol{C}(\boldsymbol{\nu})\boldsymbol{\nu} + \boldsymbol{D}(\boldsymbol{\nu})\boldsymbol{\nu} + \boldsymbol{g}(\boldsymbol{\eta}) &= \boldsymbol{\tau} \end{aligned} \quad (1.36)$$

Where:

$$\begin{aligned} \boldsymbol{M} &= \boldsymbol{M}_{rb} + \boldsymbol{M}_A \\ \boldsymbol{C} &= \boldsymbol{C}_{rb} + \boldsymbol{C}_A \end{aligned} \quad (1.37)$$

The dynamic model can be conveniently arranged like in [49] since it is convenient to present the nonlinear model in the $\dot{\boldsymbol{x}} = \boldsymbol{f}(\boldsymbol{x}, t)$ form [50].

$$\boldsymbol{M}\dot{\boldsymbol{\nu}} = -(\boldsymbol{C}(\boldsymbol{\nu})\boldsymbol{\nu} + \boldsymbol{D}(\boldsymbol{\nu}))\boldsymbol{\nu} - \boldsymbol{g}(\boldsymbol{\eta}) + \boldsymbol{\tau} \quad (1.38)$$

Since $\boldsymbol{M}^{-1}\boldsymbol{M} = \boldsymbol{I}$ (this proves that the inverse of $\boldsymbol{M}^{-1}$ exists):

$$\dot{\boldsymbol{\nu}} = \boldsymbol{M}^{-1}[-(\boldsymbol{C}(\boldsymbol{\nu}) + \boldsymbol{D}(\boldsymbol{\nu}))\boldsymbol{\nu} - \boldsymbol{g}(\boldsymbol{\eta}) + \boldsymbol{\tau}] \quad (1.39)$$

In state-space terminology, $\boldsymbol{\nu}$ is the state variables vector. Since the dynamic behavior is also dependent on the hydrostatic forces vector and, since this vector is a function of ϕ and θ, the latter are also state variables.

1.8 Purpose and Contribution

Control of AUVs is a complex challenge. This is mainly due to the variety of nonlinear hydrodynamic forces that these vehicles are subjected to. Moreover, since AUVs operate autonomously and carry a variety of very expensive equipment thus, the possibility of vehicle loss could prove costly and places extra requirements for the performance of the control system. Although modern feedback controllers are very capable, the underlying dynamic model, and therefore the validity of its parameters, can have an impact on controller performance. It is therefore paramount to devote the necessary effort for the estimation and validation of model parameters.

In this context, the purpose of this thesis is to devise the dynamic model of a AUV being developed at CEiiA - *Centro de Engenharia e Desenvolvimento de Produto*. This work is aimed at increasing CEiiA's capabilities in the field of control for underwater vehicles. The main goal of the model is the design of the control system, however, the same can be used for simulation, devising reference models for navigation and performance analysis during and after vehicle development [9, 16, 51].

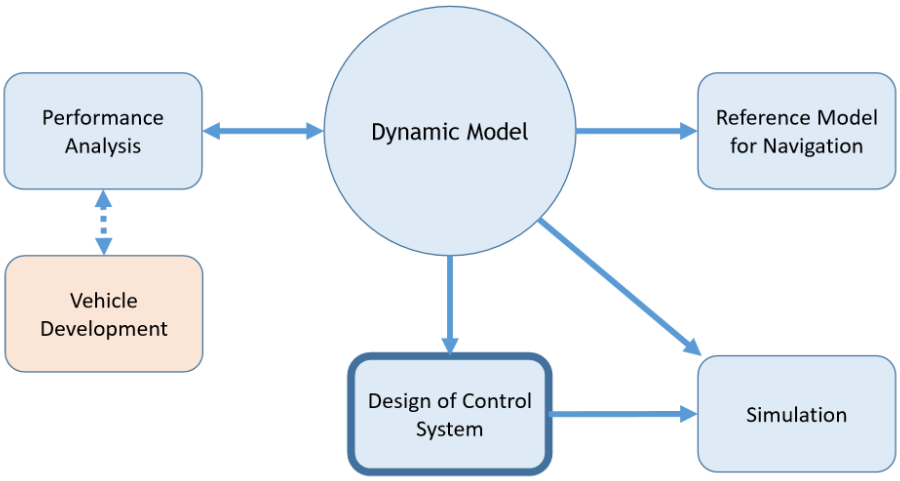

Figure 1.10: Common uses for the dynamic model.

An overview of dynamic models commonly used for underwater vehicles suggests that Fossen's dynamic model for marine craft is the most suited for modeling the AUV being developed at CEiiA. Since the main purpose is the application of control and, in the scope of providing different control design approaches, the appropriate lateral and longitudinal models are devised. These subsystems allow a) for a better understanding dynamic characteristics of the vehicle within the horizontal and vertical planes b) a simpler approach for controller design. Data estimation is achieved using analytic and computational methods. Data estimated via computational methods is provided by CEiiA and subsequently adapted to satisfy model parameters. Upon completion of the model parameters, simulation programs were devised. These programs are suited for controller design, analysis of the maneuverability and analysis of stability. The validity of the lateral and longitudinal models is also addressed using simulation.

1.9 Outline

This thesis is organized in the following manner:

- **Chapter 1** contextualizes the research developed in this thesis by providing a brief historical introduction, a description of the reference AUV, the necessary bibliographic review and other relevant topics.

- In **chapter 2** the longitudinal and lateral models are devised to meet the particularities of the considered AUV. This was performed by decoupling the lateral and longitudinal motions.

- **Chapter 3** addresses the estimation of model parameters for the AUV being developed at CEiiA using analytic and computational methods.

- **Chapter 4** validates the lateral and longitudinal models by comparing simulation results between the decoupled and the complete models. A helical diving test is also performed to study the behavior of the vehicle for coupled motion scenarios.

- **Chapter 5** expresses the conclusions derived from this research and provides guidance for further works based on this study.

Chapter 2

3DoF Subsystems

A common approach in the design of controllers for marine vehicles is to use reduced-order models (or subsystems), and desive individual control to each subsystem. This is achieved by decoupling the motions of the vehicle. For *slender body* vehicles, such as aircraft, submarine and most AUVs, it is common to devise two, slightly interacting, subsystems: the lateral and the longitudinal. 1DoF models are also common for simple control systems [9].

The usefulness of the reduced-order models is dependent on the requirements for the controller. In this context, the advantages of each of the most common subsystems, the one and three DoF subsystems, and of the complete 6DoF model, are now summarized according to [9]:

- 1DoF - Allows the implementation of control for simple motion. These models are traditionally used for forward speed and depth control and heading autopilots. Such models are simple to devise and allow the direct implementation of traditional feedback controllers.

- 3DoF - Although other 3DoF subsystems can be devised, the most common for underwater vehicles are the lateral and longitudinal subsystems. The lateral subsystem (sway, roll and yaw) is mostly used for turning and heading control. The longitudinal subsystem (surge, heave and pitch) is regularly used for forward speed, depth and pitch control. Since interaction between the subsystems is assumed to be small, the same can be used to implement simpler control systems, when compared to the complete model, without significant loss of performance.

- Complete Model - The 6DoF equations of motion capture the interaction between all DoF and are used in the design of advanced control systems, as well as for simulations.

Considering that the model being devised is the basis for the implementation of a controller, the author felt that this work would be incomplete without considering the lateral and longitudinal subsystems since they provide a different approach for such implementation. Although a simplified form of these subsystems is devised by Fossen, 2011 [9], these were found to be unsuited because they do not address the particularities of this vehicle. In this context, a more general form for the longitudinal and lateral subsystems is deduced in this chapter.

The fact that the AUV being developed at CEiiA is, essentially, the combination of two torpedo shaped bodies suggests that this decomposition is valid (validation is addressed in sections 4.2 and 4.2.1). An analysis of the 6DoF model's mass and added mass matrices shows that surge, heave and pitch are mostly dependent on the state variable in these DoFs i.e. u, w and q respectively. Complementary, sway, roll and pitch are mostly dependent on v, p and r. This is due to port/starboard symmetry of the vehicle.

Mass matrices simplification due to port/starboard symmetry accordinding to Fossen, 1994 [25]:

$$\boldsymbol{M} = \begin{bmatrix} m_{11} & 0 & m_{13} & 0 & m_{15} & 0 \\ 0 & m_{22} & 0 & m_{24} & 0 & m_{26} \\ m_{31} & 0 & m_{33} & 0 & m_{35} & 0 \\ 0 & m_{42} & 0 & m_{44} & 0 & m_{46} \\ m_{51} & 0 & m_{53} & 0 & m_{55} & 0 \\ 0 & m_{62} & 0 & m_{64} & 0 & m_{66} \end{bmatrix}$$

It is important to notice that $\mathbf{M}^{-1}\mathbf{M} = \mathbf{I}$. Also, $\boldsymbol{M}$ can be further divided into $\mathbf{M}_{long}$ and $\mathbf{M}_{lat}$:

$$\boldsymbol{M}^{long} = \begin{bmatrix} m_{11} & m_{13} & m_{15} \\ m_{31} & m_{33} & m_{35} \\ m_{51} & m_{53} & m_{55} \end{bmatrix} \qquad \boldsymbol{M}^{lat} = \begin{bmatrix} m_{22} & m_{24} & m_{26} \\ m_{42} & m_{44} & m_{46} \\ m_{62} & m_{64} & m_{66} \end{bmatrix}$$

This implies that $I_{xy} = I_{yz} = 0$, which is confirmed in section 3.2.2.

Regarding the damping matrices, the simplification applied for the mass matrices is also adopted. This yields:

$$\boldsymbol{D}^{long} = \begin{bmatrix} d_{11} & d_{13} & d_{15} \\ d_{31} & d_{33} & d_{35} \\ d_{51} & d_{53} & d_{55} \end{bmatrix} \qquad \boldsymbol{D}^{lat} = \begin{bmatrix} d_{22} & d_{24} & d_{26} \\ d_{42} & d_{44} & d_{46} \\ d_{62} & d_{64} & d_{66} \end{bmatrix}$$

This simplification is further discussed in section 3.2.5.4.

In the following sections, the influence of the remaining forces is determined.

2.1 Longitudinal Subsystem

The velocity and position vectors for the longitudinal subsystem are expressed as:

- Velocity vector - $\boldsymbol{\nu} = \begin{bmatrix} u & w & q \end{bmatrix}^T$
- Position vector - $\boldsymbol{\eta} = \begin{bmatrix} N & D & \theta \end{bmatrix}^T$

2.1.1 Longitudinal Kinematics

Assuming small angles of pitch ($\theta < 10°$), the kinematic equation for Euler angles 1.14 presented in section 1.6.1.5 can be adapted to:

$$\begin{bmatrix} \dot{N} \\ \dot{D} \\ \dot{\theta} \end{bmatrix} = \begin{bmatrix} \cos(\theta) & \sin(\theta) & 0 \\ -\sin(\theta) & \cos(\theta) & 0 \\ 0 & 0 & 1 \end{bmatrix} \begin{bmatrix} u \\ w \\ q \end{bmatrix} \quad (2.1)$$

2.1.2 Longitudinal Kinetics

The longitudinal subsystem addresses motion in surge, heave and pitch. As discussed in the beginning of this chapter, the mass and added mass suggest the surge, sway and pitch DoF are mostly dependent on corresponding states i.e. u, w and q. However, the Coriolis and hydrostatic force matrices need further analysis.

Starting with Coriolis and in accordance with [9], the Coriolis matrix due to $\boldsymbol{M}_A$ for the longitudinal subsystem multiplied by the total velocity vector $\boldsymbol{\nu} = \begin{bmatrix} u & v & w & p & q & r \end{bmatrix}^T$ is expressed as:

$$\boldsymbol{C}_{RB}^{long}(\boldsymbol{\nu})\boldsymbol{\nu} = \begin{bmatrix} m(y_g q + z_g r)p - m(x_g q - w)q - m(x_g r + v)r \\ -m(z_g p - v)p - m(z_g q + u)q + m(x_g p + y_g q)r \\ m(x_g q - w)u - m(z_g r + x_g p)v + m(z_g q + u)w + \\ (I_{yz}q + I_{xz}p - I_z r)p - (I_{xz}r - I_{xy}q + I_x p)r \end{bmatrix} \quad (2.2)$$

This clearly shows that influence of v, p and r can be significant, however, for cruise and assuming small values of v, p and r yields:

$$\boldsymbol{C}_{RB}^{long}(\boldsymbol{\nu})\boldsymbol{\nu} = \begin{bmatrix} -m(x_g q - w)q \\ -m(z_g q + u)q \\ m(x_g q - w)u + m(z_g q + u)w \end{bmatrix} = \quad (2.3)$$

$$= \begin{bmatrix} 0 & 0 & -m(x_g q - w) \\ 0 & 0 & -m(z_g q + u) \\ m(x_g q - w) & m(z_g q + u) & 0 \end{bmatrix} \begin{bmatrix} u \\ w \\ q \end{bmatrix} \quad (2.4)$$

Also, considering that $\mathbf{r}_g^b = \mathbf{0}_{3\times 1}$ (see section 3.1.2):

$$\boldsymbol{C}_{RB}^{long}(\boldsymbol{\nu})\boldsymbol{\nu} = \begin{bmatrix} 0 & 0 & mw \\ 0 & 0 & -mu \\ 0 & 0 & 0 \end{bmatrix} \begin{bmatrix} u \\ w \\ q \end{bmatrix} \quad (2.5)$$

Coriolis due to $\boldsymbol{M}_A^{long}$ for surge, heave and pitch yields:

$$\boldsymbol{C}_A^{long}(\boldsymbol{\nu})\boldsymbol{\nu} = \begin{bmatrix} -a_3 q + a_2 r \\ -a_2 p + a_1 q \\ a_3 u - a_1 w + b_3 p - b_1 q \end{bmatrix} \quad (2.6)$$

Again, assuming small values of v, p and r:

$$\boldsymbol{C}_A^{long}(\boldsymbol{\nu})\boldsymbol{\nu} = \begin{bmatrix} -a_3 q \\ a_1 q \\ a_3 u - a_1 w \end{bmatrix} = \begin{bmatrix} 0 & 0 & -a_3 \\ 0 & 0 & a_1 \\ a_3 & -a_1 & 0 \end{bmatrix} \begin{bmatrix} u \\ w \\ q \end{bmatrix} \quad (2.7)$$

Where,

$$a_1 = X_{\dot{u}} u + X_{\dot{w}} w + X_{\dot{q}} q$$
$$a_3 = Z_{\dot{u}} u + Z_{\dot{w}} w + Z_{\dot{q}} q$$

The hydrostatic force vector for the longitudinal subsystem is expressed as:

$$\boldsymbol{g}^{long}(\boldsymbol{\eta}) = \begin{bmatrix} (W - B)\sin(\theta) \\ -(W - B)\cos(\theta)\cos(\phi) \\ (z_g W - z_B B)\sin(\theta) + (x_g W - x_B B)\cos(\theta)\cos(\phi) \end{bmatrix} \quad (2.8)$$

Assuming that , $x_B = 0$ and $\mathbf{r}_g^b = \mathbf{0}_{3\times 1}$ (see section 3.1.2) and that $\phi \approx 0$, the hydrostatic force vector simplifies to:

$$\boldsymbol{g}^{long}(\boldsymbol{\eta}) = \begin{bmatrix} (W-B)\sin(\theta) \\ z_B B\cos(\theta) \\ -z_B B\sin(\theta) \end{bmatrix} \quad (2.9)$$

This shows that the longitudinal states are not only u, w and q but also θ.

The validity of the subsystem hinges on v, p, r and ϕ being and remaining small. This can be achieved by applying control to the lateral subsystem. Although the AUV of reference for this thesis is *under-actuated* (see section 3.2.6) in sway and roll, the *righting moment* is expected to correct any perturbation to the roll DoF (see section 3.2.3.1) and since the sway is mostly dependent on the effects of the lateral subsystem, it is safe to assume that, even without active control, the lateral states remain small.

The kinematic equations for the longitudinal subsystem are now expressed, in the following form:

$$\boldsymbol{M}^{long}\dot{\boldsymbol{\nu}} + \boldsymbol{C}^{long}(\boldsymbol{\nu})\boldsymbol{\nu} + \boldsymbol{D}^{long}(\boldsymbol{\nu})\boldsymbol{\nu} + \boldsymbol{g}^{long}(\boldsymbol{\eta}) = \boldsymbol{\tau}^{long} \quad (2.10)$$

Where:

$$\boldsymbol{M}^{long} = \boldsymbol{M}_{RB}^{long} + \boldsymbol{M}_{A}^{long} \quad (2.11)$$

$$\boldsymbol{C}^{long}(\boldsymbol{\nu}) = \boldsymbol{C}_{A}^{long}(\boldsymbol{\nu}) + \boldsymbol{C}_{RB}^{long}(\boldsymbol{\nu}) \quad (2.12)$$

The explicit form of the longitudinal subsystem is expressed as:

$$\begin{bmatrix} m - X_{\dot{u}} & -X_{\dot{w}} & -X_{\dot{q}} \\ -Z_{\dot{u}} & m - Z_{\dot{w}} & -Z_{\dot{q}} \\ -M_{\dot{u}} & -M_{\dot{w}} & I_y - M_{\dot{q}} \end{bmatrix} \begin{bmatrix} \dot{u} \\ \dot{w} \\ \dot{q} \end{bmatrix}$$
$$+ \begin{bmatrix} 0 & 0 & mw - (Z_{\dot{u}}u + Z_{\dot{w}}w + Z_{\dot{q}}q) \\ 0 & 0 & X_{\dot{u}}u + X_{\dot{w}}w + X_{\dot{q}}q - mu \\ Z_{\dot{u}}u + Z_{\dot{w}}w + Z_{\dot{q}}q & -(X_{\dot{u}}u + X_{\dot{w}}w + X_{\dot{q}}q) & 0 \end{bmatrix} \begin{bmatrix} u \\ w \\ q \end{bmatrix} \tag{2.13}$$
$$- \begin{bmatrix} X_u + X_{u|u|} \mid u \mid & X_w + X_{w|w|} \mid w \mid & X_q + X_{q|q|} \mid q \mid \\ Z_u + Z_{u|u|} \mid u \mid & Z_w + Z_{w|w|} \mid w \mid & Z_q + Z_{q|q|} \mid q \mid \\ M_u + M_{u|u|} \mid u \mid & M_w + M_{w|w|} \mid w \mid & M_q + M_{q|q|} \mid q \mid \end{bmatrix} \begin{bmatrix} u \\ w \\ q \end{bmatrix} + \begin{bmatrix} (W - B)\sin(\theta) \\ z_B B \cos(\theta) \\ -z_B B \sin(\theta) \end{bmatrix} = \begin{bmatrix} \tau_1 \\ \tau_3 \\ \tau_5 \end{bmatrix}$$

2.2 Lateral Subsystem

The velocity and position vectors for the longitudinal subsystem are expressed below.

- Velocity vector - $\boldsymbol{\nu} = \begin{bmatrix} v & p & r \end{bmatrix}^T$
- Position vector - $\boldsymbol{\eta} = \begin{bmatrix} N & E & \phi & \psi \end{bmatrix}^T$

2.2.1 Lateral Kinematics

For the lateral subsystem, a constant forward velocity u_k is assumed (see section 2.2.2). Thus:

$$\begin{bmatrix} \dot{N} \\ \dot{E} \\ \dot{\phi} \\ \dot{\psi} \end{bmatrix} = \begin{bmatrix} \cos(\psi) & -\sin(\psi) & 0 & 0 \\ \sin(\psi) & \cos(\psi) & 0 & 0 \\ 0 & 0 & 1 & 0 \\ 0 & 0 & 0 & 1 \end{bmatrix} \begin{bmatrix} u_k \\ v \\ p \\ r \end{bmatrix} \tag{2.14}$$

2.2.2 Lateral Kinetics

The lateral subsystem addresses motion in the sway, roll and yaw DoF. Much of the lateral subsystem can be derived in accordance with the longitudinal subsystem. However, in order

to derive the trajectory in the vertical plane, a constant forward velocity u_k was assumed. This forward velocity induces additional forces that should be considered.

The rigid-body Coriolis matrix for the sway, roll and yaw DoF is expressed as:

$$\boldsymbol{C}_{RB}^{lat}(\boldsymbol{\nu})\boldsymbol{\nu} = \begin{bmatrix} -m(y_g p + w)p + m(z_g r + x_g p)q - m(y_g r - u)r \\ -m(y_g q + z_g r)u + m(y_g p + w)v + m(z_g p - v)w \\ +(-I_{yz}q - I_{xz}p + I_z r)q + (I_{yz}r + I_{xy}p - I_y q)r \\ m(x_g r + v)u + m(y_g r - u)v - m(x_g p + y_g q)w \\ +(-I_{yz}r - I_{xy}p + I_y q)p + (I_{xz}r + I_{xy}q - I_x p)q \end{bmatrix} \quad (2.15)$$

In analogy with the longitudinal model, assuming small values of w, q and since $\mathbf{r}_g^b = \mathbf{0}_{3\times 1}$:

$$\boldsymbol{C}_{RB}^{lat}(\boldsymbol{\nu})\boldsymbol{\nu} = \begin{bmatrix} mu_k r \\ 0 \\ 0 \end{bmatrix} = \begin{bmatrix} 0 & 0 & mu_k \\ 0 & 0 & 0 \\ 0 & 0 & 0 \end{bmatrix} \begin{bmatrix} v \\ p \\ r \end{bmatrix} \quad (2.16)$$

The Coriolis force matrix due to added mass:

$$\boldsymbol{C}_{A}^{lat}(\boldsymbol{\nu})\boldsymbol{\nu} = \begin{bmatrix} a_3 p - a_1 r \\ -a_3 v + a_2 w - b_3 q + b_2 r \\ -a_2 u + a_1 v - b_2 p + b_1 q \end{bmatrix} \quad (2.17)$$

Again, assuming small values of w and q:

$$\boldsymbol{C}_{A}^{lat}(\boldsymbol{\nu})\boldsymbol{\nu} = \begin{bmatrix} a_3 p - a_1 r \\ -a_3 v + b_2 r \\ -a_2 u_k + a_1 v - b_2 p \end{bmatrix} \quad (2.18)$$

Where,

$$\begin{aligned} a_1 &= X_{\dot{u}} u_k \\ a_2 &= Y_{\dot{v}} v + Y_{\dot{p}} p + Y_{\dot{q}} q \\ a_3 &= Z_{\dot{u}} u_k \\ b_2 &= M_{\dot{u}} u_k \end{aligned}$$

This expands to:

$$\boldsymbol{C}_A^{lat}(\boldsymbol{\nu})\boldsymbol{\nu} = \begin{bmatrix} Z_{\dot{u}} u_k p - X_{\dot{u}} u_k r \\ -Z_{\dot{u}} u_k v + M_{\dot{u}} u_k r \\ -Y_{\dot{v}} v u_k + X_{\dot{u}} u_k v - M_{\dot{u}} u_k p \end{bmatrix} = \begin{bmatrix} 0 & Z_{\dot{u}} u_k & -X_{\dot{u}} u_k \\ -Z_{\dot{u}} u_k & 0 & M_{\dot{u}} u_k \\ (X_{\dot{u}} - Y_{\dot{v}}) u_k & -M_{\dot{u}} u_k & 0 \end{bmatrix} \begin{bmatrix} v \\ p \\ r \end{bmatrix} \quad (2.19)$$

The hydrostatic forces vector for the lateral subsystem is expressed as:

$$\boldsymbol{g}^{lat}(\boldsymbol{\eta}) = \begin{bmatrix} -(W - B)\cos(\theta)\sin(\phi) \\ -(y_g W - y_B B)\cos(\theta)\cos(\phi) + (z_g W - z_B B)\cos(\theta)\sin(\phi) \\ -(x_g W - x_B B)\cos(\theta)\sin(\phi) - (y_g W - y_B B)\sin(\theta) \end{bmatrix} \quad (2.20)$$

Assuming that $\theta \approx 0$, $x_B = y_B = 0$ and $\mathbf{r}_g^b = \mathbf{0}_{3\times 1}$ (see section 3.1.2). Also, since the longitudinal subsystem is responsible for depth-keeping, $B = W$ is assumed, thus, the hydrostatic force matrix for the lateral subsystem simplifies to:

$$\boldsymbol{g}^{lat}(\boldsymbol{\eta}) = \begin{bmatrix} 0 \\ -z_B W \sin(\phi) \\ 0 \end{bmatrix} \quad (2.21)$$

In analogy to the longitudinal model, the lateral subsystem requires that w, q and θ stay small and that u_k stay constant, this is achieved by applying longitudinal control. Note that all longitudinal DoFs are actively actuated.

The kinematic equations for the lateral subsystem are now expressed, in the following form:

$$\boldsymbol{M}^{lat}\dot{\boldsymbol{\nu}} + \boldsymbol{C}^{lat}(\boldsymbol{\nu})\boldsymbol{\nu} + \boldsymbol{D}^{lat}(\boldsymbol{\nu})\boldsymbol{\nu} + \boldsymbol{g}^{lat}(\boldsymbol{\eta}) = \boldsymbol{\tau}^{lat} \quad (2.22)$$

Where:

$$\boldsymbol{M}^{lat} = \boldsymbol{M}^{lat}_{RB} + \boldsymbol{M}^{lat}_{A} \quad (2.23)$$

$$\boldsymbol{C}^{lat}(\boldsymbol{\nu}) = \boldsymbol{C}^{lat}_{A}(\boldsymbol{\nu}) + \boldsymbol{C}^{lat}_{RB}(\boldsymbol{\nu}) \quad (2.24)$$

The explicit form of equation 2.22 is expressed as:

$$\begin{bmatrix} m - Y_{\dot{v}} & -Y_{\dot{p}} & -Y_{\dot{q}} \\ -K_{\dot{v}} & I_x - K_{\dot{p}} & I_{xz} - K_{\dot{q}} \\ -N_{\dot{v}} & I_{xz} - N_{\dot{p}} & I_z - N_{\dot{q}} \end{bmatrix} \begin{bmatrix} \dot{v} \\ \dot{p} \\ \dot{r} \end{bmatrix} + \begin{bmatrix} 0 & Z_{\dot{u}}u_k & mu_k - X_{\dot{u}}u_k \\ -Z_{\dot{u}}u_k & 0 & M_{\dot{u}}u_k \\ (X_{\dot{u}} - Y_{\dot{v}})u_k & -M_{\dot{u}}u_k & 0 \end{bmatrix} \begin{bmatrix} v \\ p \\ r \end{bmatrix}$$
$$- \begin{bmatrix} Y_v + Y_{v|v|} \mid v \mid & Y_p + Y_{p|p|} \mid p \mid & Y_r + Y_{r|r|} \mid r \mid \\ K_v + K_{v|v|} \mid v \mid & K_p + K_{p|p|} \mid p \mid & K_r + K_{r|r|} \mid r \mid \\ N_v + N_{v|v|} \mid v \mid & N_p + N_{p|p|} \mid p \mid & N_r + N_{r|r|} \mid r \mid \end{bmatrix} \begin{bmatrix} v \\ p \\ r \end{bmatrix} + \begin{bmatrix} 0 \\ -z_B W \sin(\phi) \\ 0 \end{bmatrix} = \begin{bmatrix} \tau_2 \\ \tau_4 \\ \tau_6 \end{bmatrix} \quad (2.25)$$

Chapter 3

Modeling the AUV

This chapter addresses the estimation of the model parameters for Fossen's dynamic model. A general description of the vehicle's dimensions and points of interest is produced to provide context and data for the estimation of parameters. Since model parameters are multi-disciplinary and, several estimation methods, of different natures, are available, a considerable effort in determining the most suitable approach for each parameter is made. In parallel with parameter estimation, the corresponding matrices of the 6DoF kinetic model are also provided. Since estimation only provides approximate values, these should be evaluated in the context of model based control. Limitations and possible solutions are subsequently discussed.

3.1 The AUV

During the development of the AUV, a detailed 3D CAD model was made by the engineers at CEiiA (see figure 3.1). The software used to produce the CAD model is *CATIA* V5 R24[1].

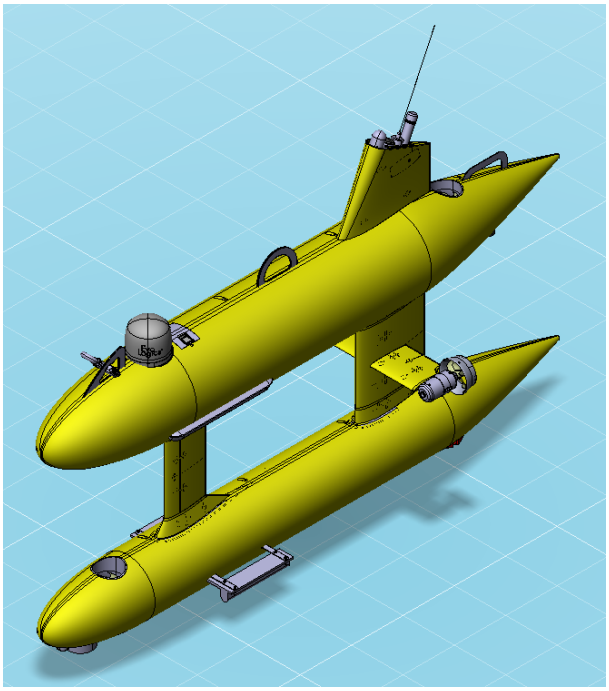

Figure 3.1: Isometric view of the AUV (courtesy of CEiiA).

[1]CATIA is a trademark of Dassault Systèmes.

3.1.1 General Dimensions

Figures 3.2, 3.3, 3.4 and 3.5 and the corresponding distances (see table 3.1) were devised using the 3D CAD model provided by CEiiA.

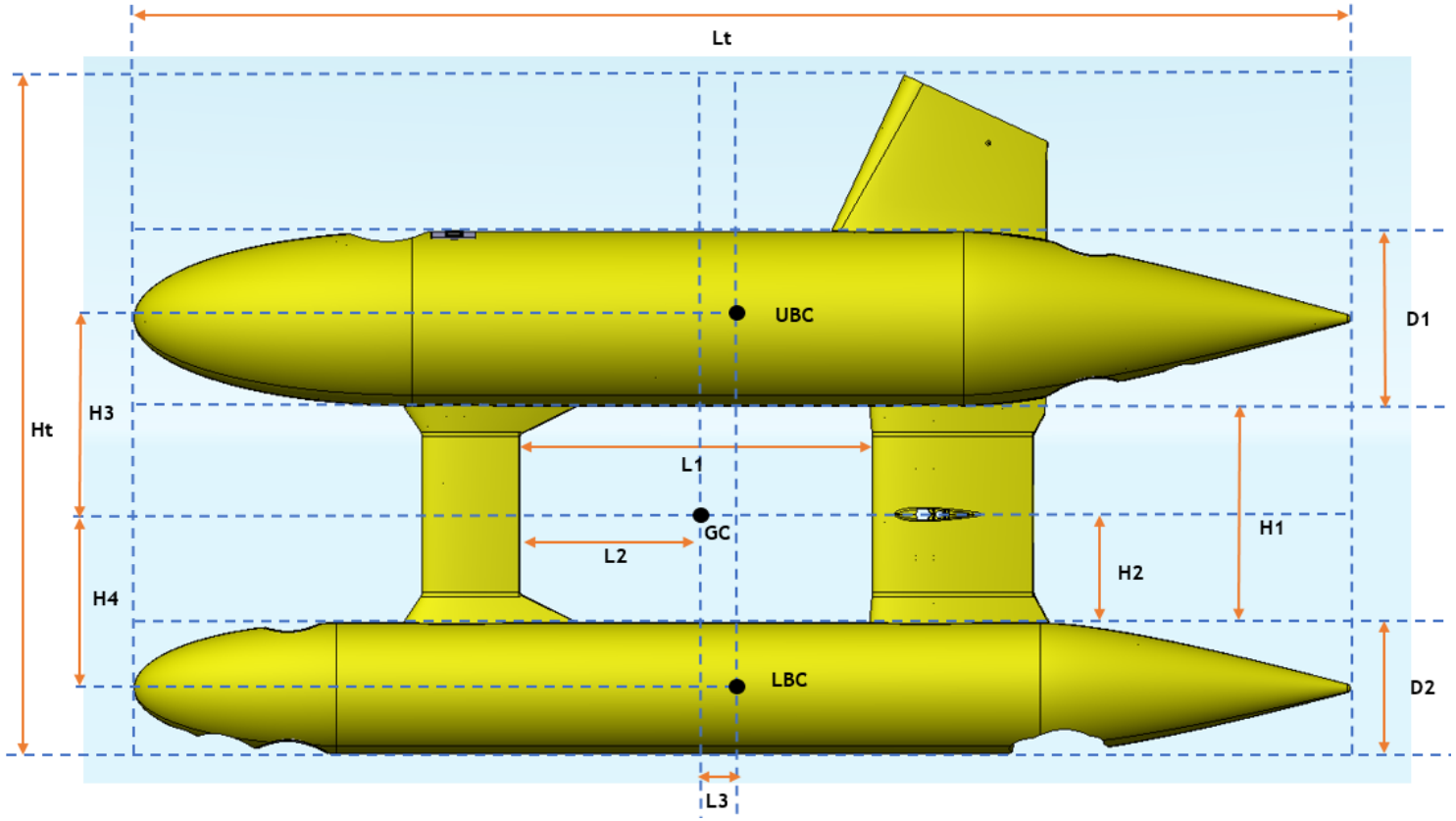

Figure 3.2: General dimensions of the AUV.
UBC - Upper Body Center.
LBC - Lower Body Center.

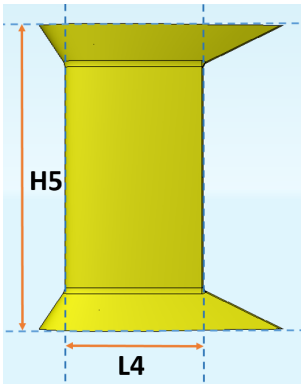

Figure 3.3: Forward fairing dimensions.

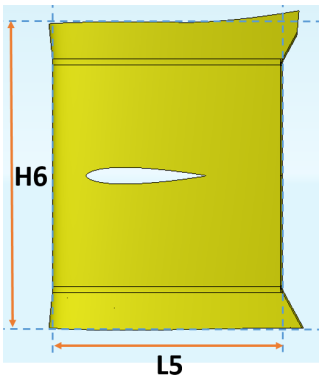

Figure 3.4: Aft fairing dimensions.

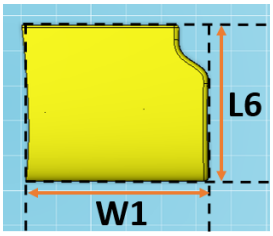

Figure 3.5: Left-hand side horizontal fairing dimensions.

Table 3.1: Dimensions for figures 3.2, 3.3, 3.4 and 3.5 (in millimeters).

D1	400
D2	300
Ht	1,563
H1	500
H2	250
H3	450
H4	400
H5	500
H6	500
Lt	2,800
L1	810
L2	386
L3	125
L4	225
L5	372
L6	200
W1	235

3.1.2 Body-Fixed Points and Reference frame

The geometric center (GC) of this vehicle is defined in the following figure.

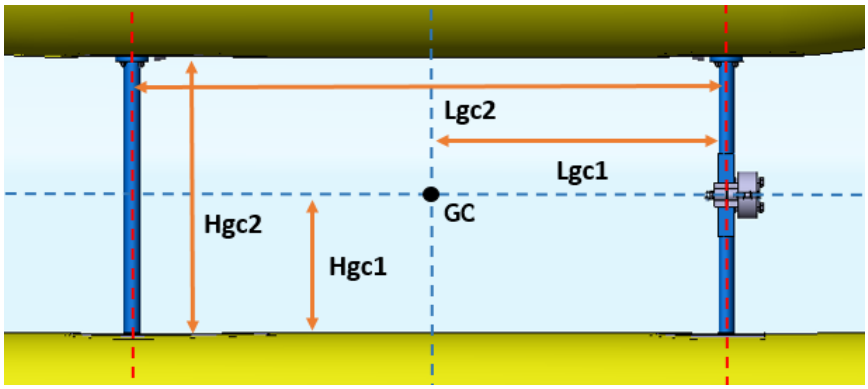

Figure 3.6: Definition of the geometric center (GC) (not to scale).

Table 3.2: Distances for figure 3.6 (in millimeters).

Lgc1	540
Lgc2	1,080
Hgc1	250
Hgc2	500

The position of CG and CB, in relation to the GC, is the sum of the individual components contribution:

$$x_g = \sum_{i=1}^{n} m_i \frac{x_i^g}{m} \quad (3.1)$$

$$x_b = \sum_{i=1}^{n} \nabla_i \frac{x_i^B}{\nabla} \quad (3.2)$$

Where x_i^g is the x coordinate of the CG of the component i, m_i is the component's mass, n is the total number of components m is the total mass of the vehicle, x_i^B is the x coordinate of the CB of component i, ∇_i volume of displaced water by component i, ∇ is the total volume of displace water. The y and z coordinates can be determined by analogy.

It is important to note that the vehicle was designed so that the GC, CG and CB are vertically aligned.

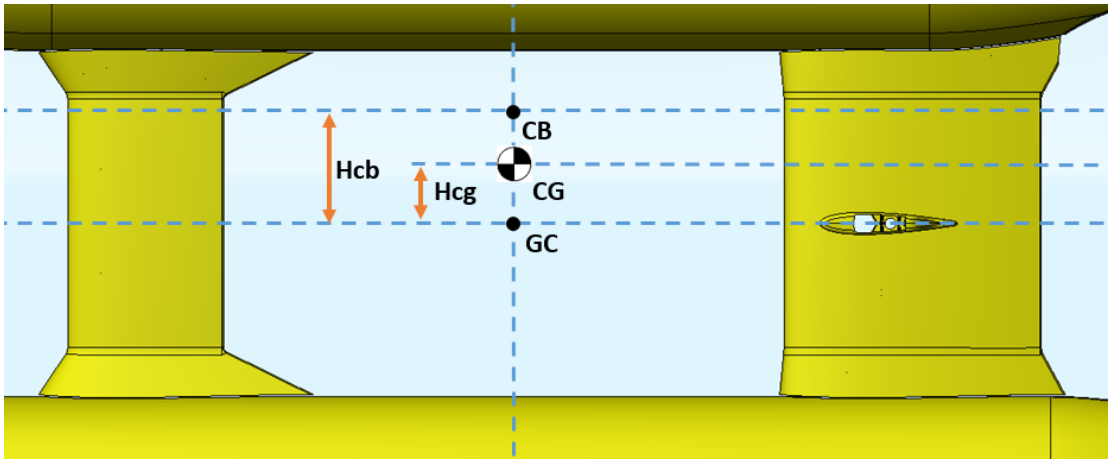

Figure 3.7: Location of geometric center (GC), CG, CB (not to scale).

Table 3.3: Distances of 3.7 (in millimeters).

Hcb	145
Hcg	71

A common simplification of the dynamic model is to assume that the origin of the body-fixed reference frame coincide with the CG i.e. $\mathbf{r}_g^b = \begin{bmatrix} 0 & 0 & 0 \end{bmatrix}^T$. This greatly simplifies the model since some elements of the rigid-body matrices are dependent on the coordinates of the CG. This simplification is adopted for the dynamic model of this vehicle. Hence:

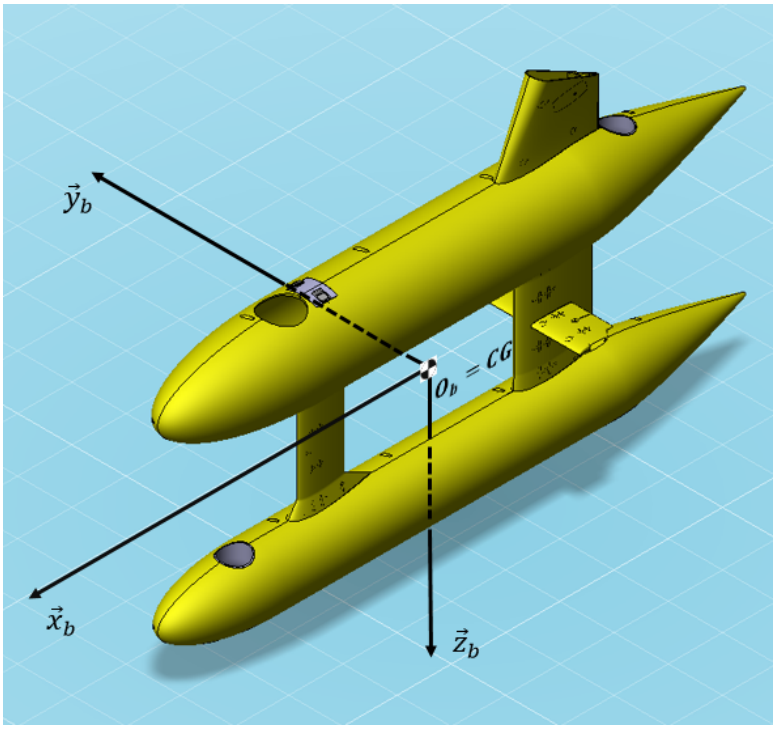

Figure 3.8: Body-fixed axis for considered vehicle (not to scale).

The location of CB in relation to the CG is given by $\mathbf{r}_B^g = \begin{bmatrix} 0 & 0 & z_B \end{bmatrix}^T$ where $z_b = -(Hcb - Hcg) = -0.074\ meters$. This distance is sometimes refereed to as the metacentric height.

3.2 Parameter Estimation

Several methods can be used to estimate the parameters of interest for an AUV. Current estimation methods can be divided into experimental, analytical, computational [52]. The traditional approach in estimating dynamic parameters is to combine analytical and experimental methods [53]. Computational methods are becoming more popular, namely for hydrodynamic estimation. These allow for fast estimation without the need for experimental tests, therefore reducing costs (see [52] and [54]). A recent exprerimental method, worth mentioning, is system identification. This works by applying a known control input to the vehicle and measuring accelerations. The resulting force and moment parameters are subsequently integrated [45, 55]. The advantage of this method is the short time required for estimation, which can be performed, for instance, in the early stage of the mission. However, performing systems identification requires a dynamic model, even if it is a simplified one[45].

Due to a multitude of methods available, vehicle particularities, and current state of the project, some sort of criteria to choose the best approach should be devised.

3.2.1 Criteria and Considerations

Considering the data acquisition stage of the proposed mission scenarios for this AUV (see section 1.3.1) and the particularities of this vehicle, the following considerations should be taken into account for the estimation of model parameters.

- *Extreme maneuvers are not expected.*
- *Static stability is assured by the metacentric height* (see section 3.2.3).
- *Principle direction of motion is forward.*

Having into account this considerations and current limitations, the following criteria for choosing estimation methods was devised. The estimation method should:

- be applicable for multi-component vehicles.
- provide accurate results.
- provide results in a time-efficient manner.
- be of non-experimental nature.

Although most methods do not satisfy all the criteria stated above, an effort is made to employ the most suitable approach.

3.2.2 Rigid-body Parameters

The rigid-body matrices parameter are mass and inertia. The mass and inertia parameters are cumulative, meaning that the total mass/inertia is the sum of the individual components mass/inertia.

The vehicle is designed so that the only components that do not present hydrostatic pressure equilibrium are the pressure hulls, necessary due to the fragile nature of the payload. This implies that water infiltrates the vehicle's interior and, since this water moves with the vehicle, its mass and inertia should also be considered. The mass of the submerged vehicle is addressed as *wetted mass*. The mass of the vehicle "in air" is denoted as *dry mass*. The mass of a component is given by the multiplication of its volume by its density:

$$m_i = V_i \rho_i \quad (3.3)$$

The dry and wetted masses were determined using the following expressions, respectively:

$$m_{dry} = \sum_{i=1}^{n} m_i \quad (3.4)$$

$$m_{wet} = m_{dry} + m_{vw} \quad (3.5)$$

The general formula for the *moment of inertia of a three-dimentional homogeneous body*, with respect to a coordinate axis, can be found in [40] and is expressed as:

$$I = \rho \int r^2 dV \quad (3.6)$$

For complex geometries it is necessary to perform double or triple integration, thus, the inertial parameters for AUVs are traditionally modeled using simplified shapes. A recent approach is to use the CAD model to determine inertial parameters.

Using equation 3.6 and defining the CG of this vehicle as the center of the inertial system, the CAD software is able to determine the resulting inertial parameters.

At this moment in the stage of the project, not all mass parameters are defined in the CAD model, thus, the components that can be estimated using computational methods are: the

main stucture (figure 3.9); the syntactic foam; the electronics (payload of the upper pressure hull) and the batteries (payload of the lower pressure hull).

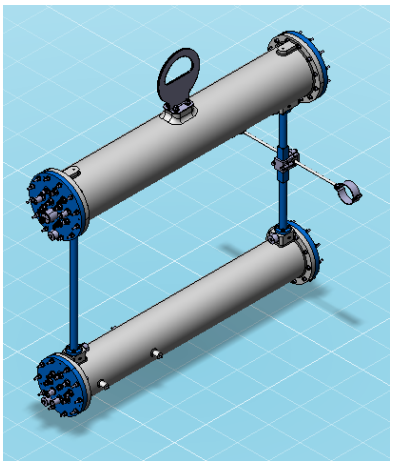

Figure 3.9: Isometric view of the main structure.

The contribution of the remaining components (sensors, fairings, motors, supports, cables and ascent weight) are determined using the formula for the *moment of inertia of a point mass*:

$$I = mr^2 \quad (3.7)$$

Which expands to:

$$\begin{aligned} I_x &= m(y^2 + z^2) \\ I_y &= m(x^2 + z^2) \\ I_z &= m(x^2 + y^2) \end{aligned} \quad (3.8)$$

The remaining components are denoted as *other components* hereinafter.

Table 3.4: Mass [kg] and Inertia [$kg \cdot m^2$] for this vehicle.

Component	Mass	I_{xx}	I_{yy}	I_{zz}	I_{xz}
Main structure	96.03	12.88	25.88	14.08	-0.10
Upper syntactic foam	55.56	10.42	22.03	13.01	-2.44
Lower syntactic foam	22.76	5.00	7.89	3.23	0.38
Upper hull electronics	8.83	0.95	1.94	1.03	-0.28
Batteries	21	5.22	7.30	2.14	0.00
Other components	107.85	23.89	83.66	60.55	*unknown*
In-vehicle water	128.5	*unknown*	*unknown*	*unknown*	*unknown*
TOTAL	440.48	58.35	148.71	94.04	-2.44

The inertia parameters in table 3.4 were determined in relation to the CG. Note that the contribution of in-vehicle water to inertia is not considered. Further discussion can be found in section 3.3.

3.2.2.1 Rigid Body Mass Matrix for the Complete Model

Applying the estimations in table 3.4 to equation 1.17 yields:

$$\mathbf{M}_{rb} = \begin{bmatrix} 440.48 & 0 & 0 & 0 & 0 & 0 \\ 0 & 440.48 & 0 & 0 & 0 & 0 \\ 0 & 0 & 440.48 & 0 & 0 & 0 \\ 0 & 0 & 0 & 58.35 & 0 & 2.44 \\ 0 & 0 & 0 & 0 & 148.71 & 0 \\ 0 & 0 & 0 & 2.44 & 0 & 94.04 \end{bmatrix} \quad (3.9)$$

3.2.3 Hydrostatic Forces

The hydrostatic forces are modeled considering the total weight and buoyant forces and the position of the respective centers i.e. the CG and the CB. The location of these centers is addressed in section 3.1.2.

A typical practice in designing UUVs is to adjust the total so that the vehicle attains residual buoyancy. This ensures that, if control is lost, the vehicle will eventually surface. This is also the case for this vehicle.

The weight and buoyant forces are the sum of the individual components contribution:

$$B = \rho g \sum_{i=1}^{n} \nabla_i = 1027 \times 9.807 \times 0.30674 \approx 3,089\ N$$

$$W = g \sum_{i=1}^{n} m_i = 9.807 \times 312.019 \approx 3,060\ N$$

Where $\rho = 1027\ kg/m^3$ is the density of salt-water, $g = 9.807\ m/s$ is the acceleration of gravity, $\sum_{i=1}^{n} \nabla_i \simeq 0.30674\ m^3$ is the total volume of water displaced by the vehicle and $\sum_{i=1}^{n} m_i \simeq 312\ kg$ is the vehicle's *dry mass*. The net buoyancy ($B - W$) is $\simeq 29\ N$.

3.2.3.1 Contribution to Stability

The weight force acts on the CG and always points to the center of the Earth. The buoyant force acts upon the CB, in the opposite direction of the weight force. If the CG and CB are not aligned (non zero angle of attack or pitch), a positive metacentric height induces a righting moment.

In *Stability and buoyancy*[2] [56], the minimum values of the metacentric height for sufficient stability are provided. For a submerged underwater vehicle this distance is 0.05 meters. Since the metacentric height for the considered AUV is 0.074 meters, static stability of pitch and roll is assumed.

3.2.3.2 Hydrostatic Forces Vector

The hydrostatic forces vector differs depending on the method used for vector transformation. In this context, two hydrostatic force vectors are presented for quaternions and for euler angle transformation.

[2] Norm form DNV GL.

- **Hydrostatic force vector - Quaternions**

  The hydrostatic force vector if using quaternions is found in section 1.6.2.2 by equation 1.25. Since $\mathbf{r}_g^b = \mathbf{0}_{3\times 1}$, equation 1.25 expands to:

$$\boldsymbol{g}(\boldsymbol{\eta}) = - \begin{bmatrix} 2(W-B)(q_1 q_3 - q_2 q_0) \\ 2(W-B)(q_2 q_3 + q_1 q_0) \\ (W-B)(1-2(q_1^2+q_2^2)) \\ 2z_b B(q_2 q_3 + q_1 q_0) \\ -2z_b B(q_1 q_3 - q_2 q_0) \\ 0 \end{bmatrix} \quad (3.10)$$

  Applying the weight and buoyant force and z_b of this vehicle yields:

$$\boldsymbol{g}(\boldsymbol{\eta}) = \begin{bmatrix} -58(q_1 q_3 + q_2 q_0) \\ -58(q_2 q_3 + q_1 q_0) \\ -29(1-2(q_1^2+q_2^2)) \\ 457(q_2 q_3 + q_1 q_0) \\ -457(q_1 q_3 + q_2 q_0) \\ 0 \end{bmatrix} \quad (3.11)$$

- **Hydrostatic force vector - Euler**

  Again, since $\mathbf{r}_g^b \mathbf{0}_{3\times 1}$ and applying the vehicle's weight and buoyant force, the hydrostatic force vector, defined by equation 1.6.2.2, simplifies to:

$$\boldsymbol{g}(\boldsymbol{\eta}) = \begin{bmatrix} -29 \cdot \sin(\theta) \\ 29 \cdot \cos(\theta)\sin(\phi) \\ 29 \cdot \cos(\theta)\cos(\phi) \\ -229 \cdot \cos(\theta)\sin(\phi) \\ -229 \cdot \sin(\theta) \\ 0 \end{bmatrix} \quad (3.12)$$

  Since the vertical thrusters can compensate for the residual buoyancy in depth-keeping, it is common to assume $B = W \simeq 3,060\ N$. This assumption yields:

$$\boldsymbol{g}(\boldsymbol{\eta}) = \begin{bmatrix} 0 \\ 0 \\ 0 \\ -226.4 \cdot \cos(\theta)\sin(\phi) \\ -226.4 \cdot \sin(\theta) \\ 0 \end{bmatrix} \quad (3.13)$$

This assumption was adopter for simulations purposes.

3.2.4 Added mass

Added mass is a complex phenomena that is challenging to model correctly, however, as discussed in section 1.6.2.3, several methods are available. Since computational methods using CFD are still recent and specialized programs are not available, analytic methods are explored. In [57] analytic expressions can be found for simple body shapes and, in [43], expressions for estimating added mass of multi-component vehicle via ellipsoid approximation are presented. Both methods meet all criteria for modeling methods except that results may be over simplistic since that body simplification must be carried out in the interest of time-efficiency. In this context, Watts method [43] is used for estimating the added mass contribution of the upper and lower bodies and, for the contribuition of the hydrodynamic fairings (both horizontal and vertical), Newman's methode [57] is used. Interference between the hydrodynamic fairings and the hulls is also neglected. Due to the geometrical simplifications, results are assumed to be underestimated. Further discussion in section 3.3.

3.2.4.1 Added Mass for the Hydrodynamic Fairings

For an horizontal flat plate, added mass can be expressed in accordance with [30] and [57].

$$\begin{aligned} Z_{\dot{w}} &= \frac{1}{4}\pi\rho\ chord^2\ span \\ M_{\dot{q}} &= Z_{\dot{w}}\bar{x}^2 \\ Z_{\dot{q}} &= M_{\dot{w}} = Z_{\dot{w}}\bar{x} \end{aligned} \quad (3.14)$$

Where $\bar{x}$ is the length in the longitudinal DoF from $1/3\ chord$ to O_B and $\rho = 1027\ kg/m^3$ is the density of salt-water.

For a vertical flat plate, added mass can be expressed as:

$$\begin{aligned} Y_{\dot{v}} &= \frac{1}{4}\pi\rho\ chord^2\ span \\ N_{\dot{r}} &= Y_{\dot{v}}\bar{y}^2 \\ Y_{\dot{r}} &= N_{\dot{v}} = Y_{\dot{v}}\bar{y} \end{aligned} \tag{3.15}$$

Where $\bar{y}$ is the length in the longitudinal DoF from $1/3\ chord$ to O_B and $\rho = 1020\ kg/m^3$ is the density of water.

Contribution to roll is neglected in both cases.

- Horizontal hydrodynamic fairings:
  The chord and span are defined in figure 3.5 and $\bar{x}$ is defined in figure 3.6. This yields:

  $Z_{\dot{w}} = -65.03\ kg$
  $M_{\dot{q}} = -16.26\ kgm^2$
  $Z_{\dot{q}} = M_{\dot{w}} = -32.51\ kgm$

- Forward vertical hydrodynamic fairings:
  The chord and span are defined in figure 3.3 and $\bar{x}$ is defined in figure 3.6.

  $Y_{\dot{v}} = -41.06\ kg$
  $N_{\dot{r}} = -12\ kgm^2$
  $Y_{\dot{r}} = N_{\dot{v}} = -22.17\ kgm$

- Aft vertical hydrodynamic fairings:
  The chord and span are defined in figure 3.4 and $\bar{x}$ is defined in figure 3.6.

  $Y_{\dot{v}} = -55.43\ kg$
  $N_{\dot{r}} = -32.47\ kgm^2$
  $Y_{\dot{r}} = N_{\dot{v}} = 60.14\ kgm$

3.2.4.2 Added Mass for the Upper and Lower Bodies

In accordance with [43], for an ellipsoid where the semi-major axis is represented by a and semi-minor axis by b and c, the added mass parameters are expressed as:

$$
\begin{aligned}
X_{\dot{u}} &= -\rho V t_{11} \\
X_{\dot{q}} &= \bar{z} X_{\dot{u}} \\
X_{\dot{r}} &= -\bar{y} X_{\dot{u}} \\
Y_{\dot{v}} &= -\rho V t_{22} \\
Y_{\dot{p}} &= -\bar{z} Y_{\dot{v}} \\
Y_{\dot{r}} &= \bar{y} Y_{\dot{v}} \\
Z_{\dot{w}} &= -\rho V t_{33} \\
Z_{\dot{p}} &= \bar{y} Z_{\dot{w}} \\
Z_{\dot{q}} &= -\bar{x} Z_{\dot{w}} \\
K_{\dot{p}} &= -\rho V t_{44} + \bar{y}^2 Z_{\dot{w}} + \bar{z}^2 Y_{\dot{v}} \\
K_{\dot{q}} &= -\bar{y}\bar{x} Z_{\dot{w}} \\
K_{\dot{r}} &= -\bar{x}\bar{z} Y_{\dot{v}} \\
M_{\dot{q}} &= -\rho V t_{55} + \bar{z}^2 X_{\dot{u}} + \bar{x}^2 Z_{\dot{w}} \\
M_{\dot{r}} &= -\bar{y}\bar{z} X_{\dot{u}} \\
N_{\dot{r}} &= -\rho V t_{66} + \bar{x}^2 Y_{\dot{v}} + \bar{y}^2 X_{\dot{u}}
\end{aligned}
\tag{3.16}
$$

Where V is the volume of an ellipsoid $V = 3/4(\pi\ a\ b\ c)$ and $\bar{x}$, $\bar{y}$ and $\bar{z}$ are the body-fixed coordinates of the center of the ellipsoid i.e. UBC and LBC, as defined in figure 3.2. The parameters $t_{11}, ..., t_{66}$ are expressed as:

$$
\begin{aligned}
t_{11}(a,b,c) &\sim \frac{bc}{a^2}(\Lambda - 1) + \frac{bc}{4a^4}\left[\Lambda(4bc\Lambda + 3c^2 - 8cb + 3b^2) - 4c^2 + 7cb - 4b^2\right] \\
t_{22}(a,b,c) &\sim \frac{c}{b} - \frac{c(c+b)}{4a^4 b}\left[2(c+b)\Lambda - c - 3b\right] \\
&\quad + \frac{c(c+b)}{64a^4 b}\left\{4(c+b)\Lambda\left[4c(c+b)\Lambda - 7c^2 - 12cb - 9b^2\right] + 17c^3 + 25c^2 b + 51c^2 b + 51b^3\right\} \\
t_{33} &= t_{22}(a,c,b) \\
t_{44}(a,b,c) &\sim \frac{(c^2 - b^2)^2}{10bc}\left\{1 - \frac{(c+b)^2}{4a^2} + \frac{(c+b)^2}{64a^4}\left[12(c+b)^2\Lambda - 15c^2 - 26cb + 15b^2\right]\right\} \\
t_{55}(a,b,c) &\sim \frac{ba^2}{5c} - \frac{b}{20c}\left[6(c+b)^2\Lambda - 3c^2 - 20cb - 5b^2\right] \\
&\quad + \frac{b}{320a^2 c}\{12(c+b)^2\Lambda\left[12(c+b)\Lambda + c^2 - 60cb - 25b^2\right] \\
&\qquad + 3c^4 + 598c^3 b + 1468c^2 b^2 + 794cb^3 + 177b^4\} \\
t_{66} &= t_{55}(a,c,b)
\end{aligned}
\tag{3.17}
$$

Where:

$$\Lambda \equiv \ln(\frac{4a}{c+b})$$

The method presented in [43] requires body approximation by ellipsoid. This was performed with semi-major axis $a = length/2$ and semi-minor axis $b = c = diameter/2$, for each hull. The length and diameter of each body can be found in figure 3.2. The coordinates of the UBC and LBC (with respect to the CG) are deduced from figure 3.2 and 3.7. These results are summarized in the following tables:

Table 3.5: Distance parameter for upper body.

Parameter	distance [mm]
a	1,400
$b = c$	200
$\bar{x}$	-125
$\bar{y}$	0
$\bar{z}$	-376

Table 3.6: Distance parameter for lower body.

Parameter	distance [mm]
a	1,400
$b = c$	150
$\bar{x}$	-125
$\bar{y}$	0
$\bar{z}$	474

Applying these distance parameters to equations 3.17 yields:

Table 3.7: Parameters for added mass estimation of the upper body.

t_{11}	0.036
t_{22}	0.940
t_{33}	0.940
t_{44}	0
t_{55}	0.354
t_{66}	0.354

Table 3.8: Parameters for added mass estimation of the lower body.

t_{11}	0.023
t_{22}	0.960
t_{33}	0.960
t_{44}	0
t_{55}	0.351
t_{66}	0.351

Finally, applying these results to equations 3.16 yields:

Table 3.9: Total added mass estimation for the upper body.

$X_{\dot{u}} = -8.54\ kg$	$Y_{\dot{r}} = 28.11\ kgm$
$X_{\dot{q}} = 3.21\ kgm$	$Z_{\dot{w}} = -224.91\ kg$
$Y_{\dot{v}} = -224.91\ kg$	$Z_{\dot{q}} = -28.11\ kgm$
$Y_{\dot{p}} = -84.57\ kgm$	$K_{\dot{p}} = -31.80\ kgm^2$
$K_{\dot{r}} = 10.57\ kgm^2$	$M_{\dot{q}} = -89.39\ kgm^2$
$N_{\dot{r}} = -88.19\ kgm^2$	

Table 3.10: Total added mass estimation for the lower body.

$X_{\dot{u}} = -3.10\ kg$	$Y_{\dot{r}} = 16.15\ kgm$
$X_{\dot{q}} = -1.47\ kgm$	$Z_{\dot{w}} = -129.19\ kg$
$Y_{\dot{v}} = -129.19\ kg$	$Z_{\dot{q}} = -16.15\ kgm$
$Y_{\dot{p}} = 61.23\ kgm$	$K_{\dot{p}} = -29.03\ kgm^2$
$K_{\dot{r}} = -7.65\ kgm^2$	$M_{\dot{q}} = -49.91\ kgm^2$
$N_{\dot{r}} = -49.21\ kgm^2$	

3.2.4.3 Added Mass Matrix

The total added mass force for the vehicle is the sum of all components added mass. Finally, the added mass matrix for this AUV can be devised:

$$\boldsymbol{M}_A = \begin{bmatrix} -11.64 & 0 & 0 & 0 & 1.74 & 0 \\ 0 & -450.58 & 0 & -23.33 & 0 & 82.23 \\ 0 & 0 & -419.13 & 0 & -76.78 & 0 \\ 0 & -23.33 & 0 & -60.82 & 0 & 2.92 \\ 1.74 & 0 & -76.78 & 0 & -155.56 & 0 \\ 0 & 82.23 & 0 & 2.92 & 0 & -181.84 \end{bmatrix} \quad (3.18)$$

The effect of underestimating the added mass coefficients in the context of control is discussed in section 3.3.

3.2.5 Hydrodynamic Damping

Estimating hydrodynamic without experimental tests is very difficult [58]. Moreover, experimental tests are usually expensive and time consuming since towing tank experiments are required. According to Conte et al, 2004 [45], theoretical derivation of damping coeficients is ”almost impossible” and, although analytic formulas are available (see [57]), these are only valid for very simple shapes which are generally unrealistic. At this moment,

there is no consensus for modeling hydrodynamic forces within the control community [16]. Continuous advances in computational methods are changing the way hydrodynamic estimations are performed. CFD analysis is proving capable of providing estimates in a time-efficient manner. In this context, and taking advantage of CEiiA's computational capabilities[3], the following method was devised for estimating damping parameters that arise from linear velocities i.e. the parameters of the first three columns of D_l and D_q). The method is described in sections 3.2.5.1 and 3.2.5.2.

3.2.5.1 Damping due to a forward velocity

The hydrodynamic force and moments that arise from motion in surge were determined using CFD analysis, by the engineers at CEiiA, for various values of forward velocity. Using this data, a quadratic curve fitting function was devised. The corresponding results are expressed in the following figures.

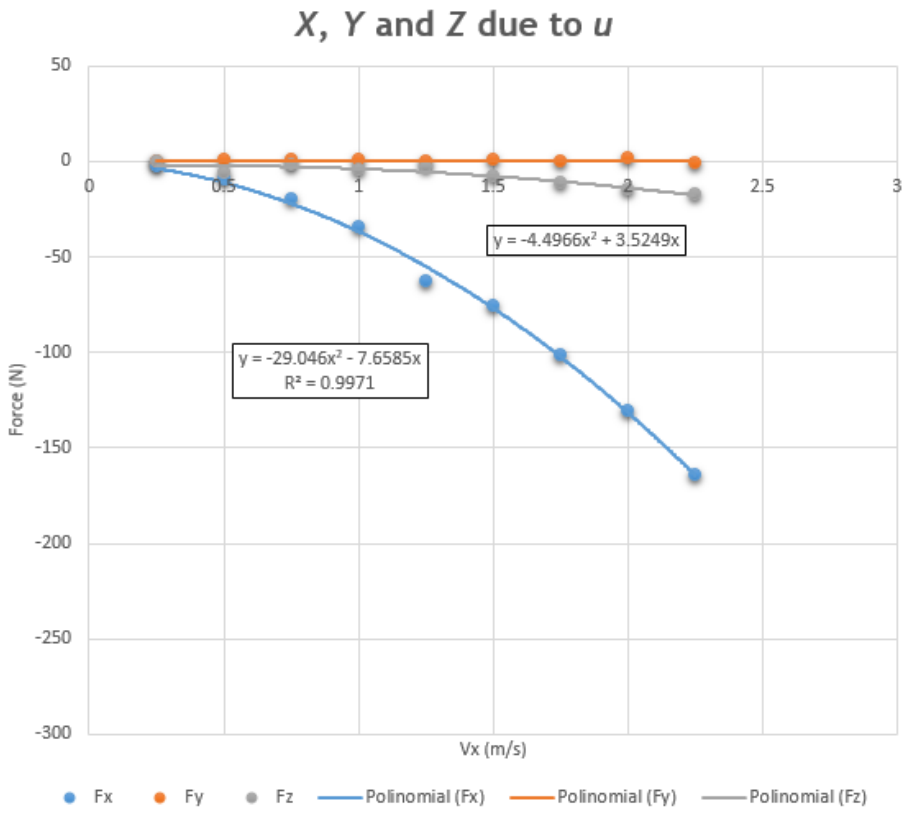

Figure 3.10: Static damping forces as a result of motion in surge.

[3]CFD analysis were performed using *Fluent 16.0*. Fluent is a product of ANSYS, Inc.

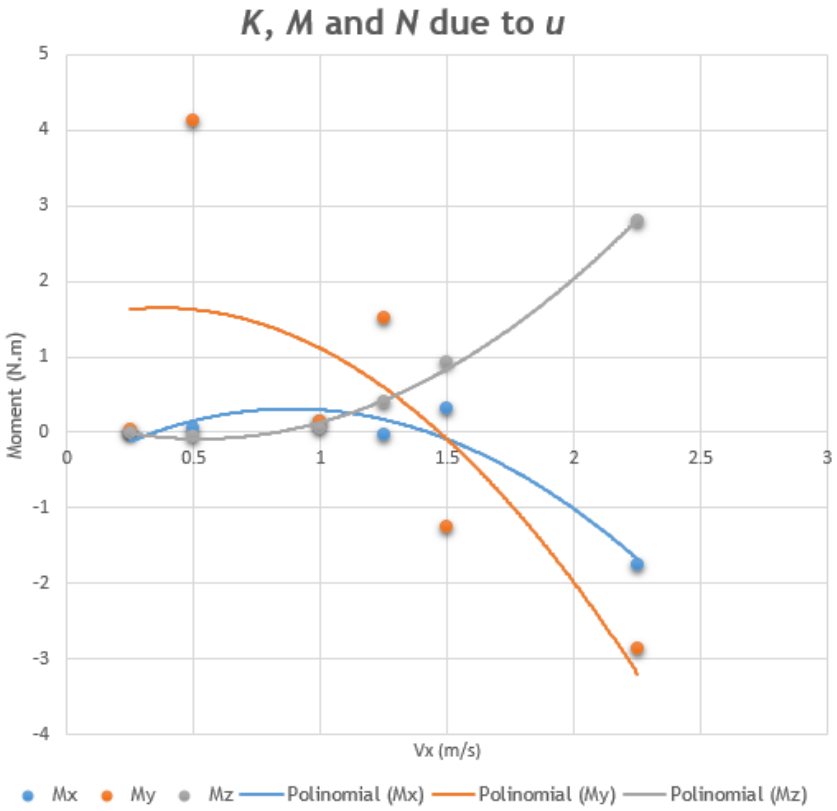

Figure 3.11: Static damping moments as a result of motion in surge.

In figure 3.10 it is clear that the dominant force is in the the longitudinal direction. A lift (since it is perpendicular to the flow) force is also present in heave, probably due to the geometric difference between the upper and lower bodies. The hydrodynamic force in sway is negligible due to symmetry in the xz plane.

The damping induced moments, expressed in figure 3.11, are negligible. Fluctuation in the values is probably due to instability in the flow. It should be noted that a pitching moment was expected due to relative sizes of the upper and lower bodies, however since moments were determined in relation to the CG, the difference in sizes, and thus damping, of both bodies is probably balanced by the respective distances to the CG. The approximated coefficients are expressed in the following tables.

Table 3.11: Linear damping coefficients for motion in surge.

$$
\begin{aligned}
X_u &= -7.66 \\
Y_u &= 0 \\
Z_u &= 3.53 \\
K_u &= 0 \\
M_u &= 0 \\
N_u &= 0
\end{aligned}
$$

Table 3.12: Quadratic damping coefficients for motion in surge.

$$
\begin{aligned}
X_{u|u|} &= -29.05 \\
Y_{u|u|} &= 0 \\
Z_{u|u|} &= -4.5 \\
K_{u|u|} &= 0 \\
M_{u|u|} &= 0 \\
N_{u|u|} &= 0
\end{aligned}
$$

3.2.5.2 Damping due to velocity in sway and heave

These hydrodynamic forces and moments were also estimated using data from CFD simulations provided by CEiiA. The simulation was performed at a given velocity for various angles of attack and side-slip (positive and independently). The results are then extrapolated, at each velocity, to $\alpha = 90^\circ$ and $\beta = 90^\circ$. A quadratic curve fitting function, as a function of velocity velocity, is subsequently devised.

It should be noted that damping for positive or negative angles of side-slip should be identical because the vehicle is symmetric in the xz plane and, although this is not the case for the xy plane, damping for positive and negative angles of attack are considered equal since CFD analysis were only performed for positive angles of attack. Moreover, the damping matrices (equations 1.33 and 1.34) assume that the superposition principle is valid i.e. damping for a given AoA or side-slip is the sum of the damping contribution in each DoF. Although this principle is used for most AUV dynamic models found in literature, for most cases, it fail to capture all hydrodynamic phenomena. However, since damping coefficients are extrapolated from the analysis performed for relatively small AoA and side-slip and, the vehicle is expect to operate in small AoA and side-slip, this method allows a better understanding of the hydrodynamic characteristics within the vehicle's operating regime. Since CFD analysis were only performed for angles smaller than 25°, the envelope of angle of attack and side-slip to which the following coefficients are to be considered valid is expressed below:

$$-25^\circ < \alpha < 25^\circ$$
$$-25^\circ < \beta < 25^\circ$$

Note that the vehicle is design to operate within this envelope. The corresponding results are now expressed by the following figures, first regarding motion in sway and then regarding motion in heave.

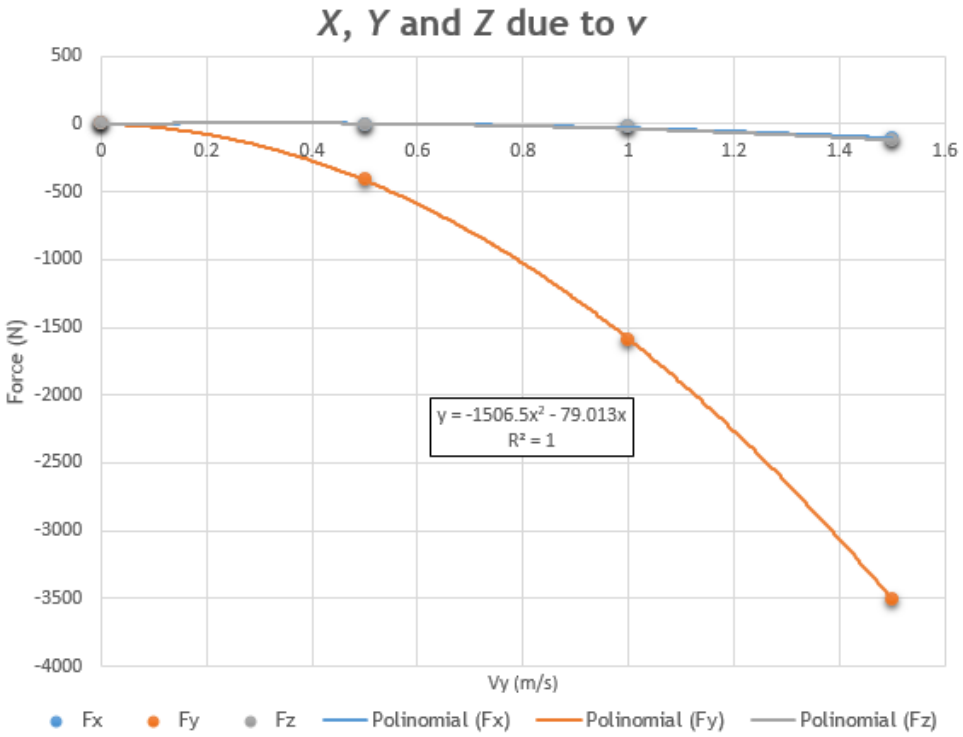

Figure 3.12: Static damping forces as a result of motion in sway.

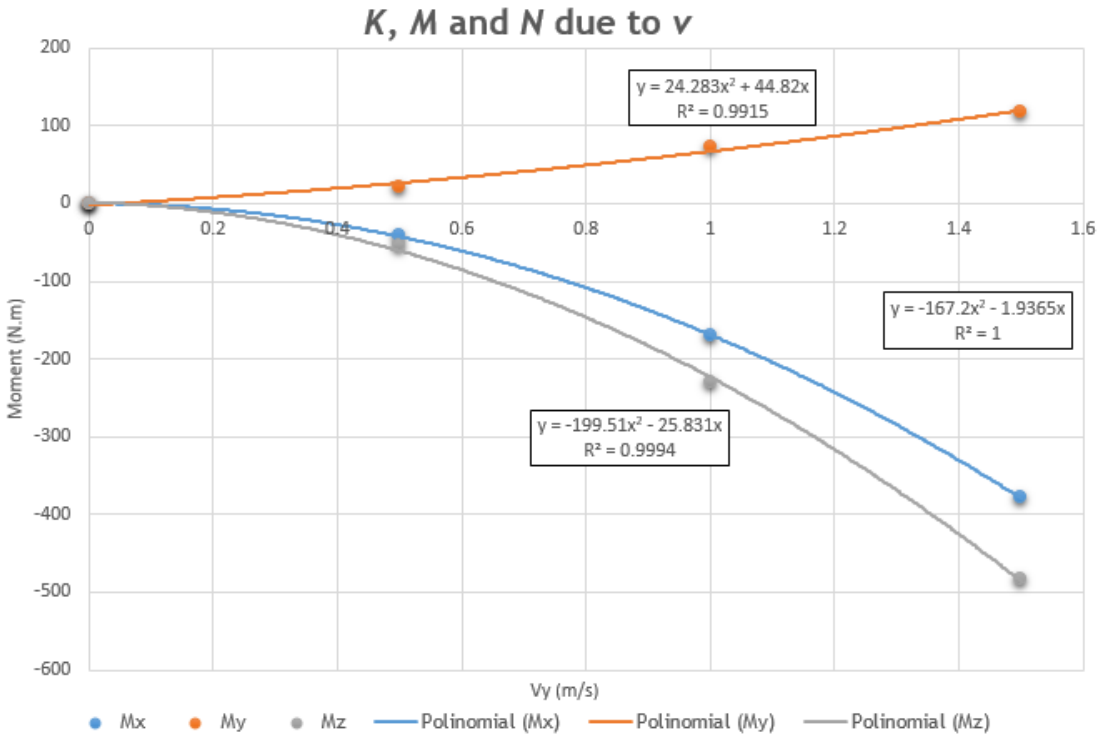

Figure 3.13: Static damping moments as a result of motion in sway.

Figure 3.12 demonstrates that forces in surge and heave are negligible. As expected, due to the large lateral area, the damping force in sway is considerable.

The damping moments, expressed in figure 3.13, presented some unexpected results. The pitching moment due to motion in sway was expected to remain very small however, and although this moment is smaller than the moments in roll and yaw, it should not be neglected. This moment is probably due to lift forces induced by some external component of the vehicle. Also, the vehicle was designed so that the aft vertical and antenna hydrodynamic fairing would produce a corrective moment in yaw and, although the corrective moment is certainly present, the CFD simulations suggest that the overall moment is destabilizing[4], however, since lateral velocity is expected to stay small, the subsequent forces and moments should also stay small. Moreover, rotation damping due to yaw i.e. N_r and $M_{r|r|}$ (see section 3.2.5.3) is expected to counterbalance the destabilizing moment.

Table 3.13: Linear damping coefficients for motion in sway.

$X_v = 0.00$	
$Y_v = -79.01$	
$Z_v = 0.00$	
$K_v = -1.94$	
$M_v = 44.82$	
$N_v = -25.83$	

Table 3.14: Quadratic damping coefficients for motion in sway.

$X_{v\|v\|} = 0.00$	
$Y_{v\|v\|} = -1506.5$	
$Z_{v\|v\|} = 0.00$	
$K_{v\|v\|} = -167.2$	
$M_{v\|v\|} = 24.28$	
$N_{v\|v\|} = -199.51$	

The hydrodynamic forces and moments due to motion in heave is expressed in the figures 3.14 and 3.15.

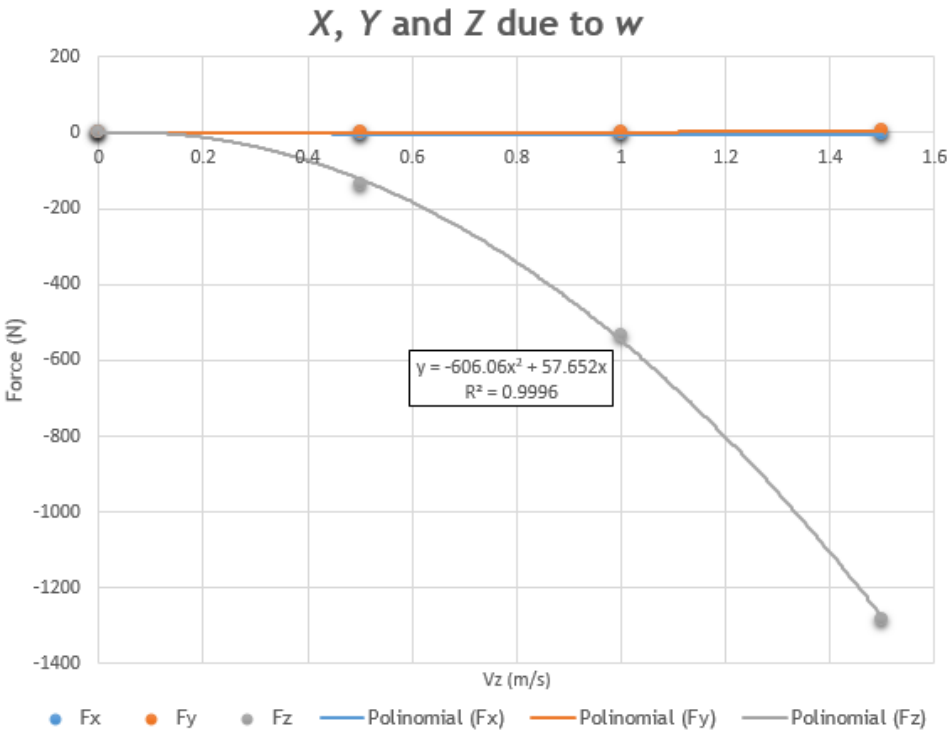

Figure 3.14: Static damping forces as a result of motion in heave.

[4]Meaning that the vehicle ”turns” in the direction opposite to the flow

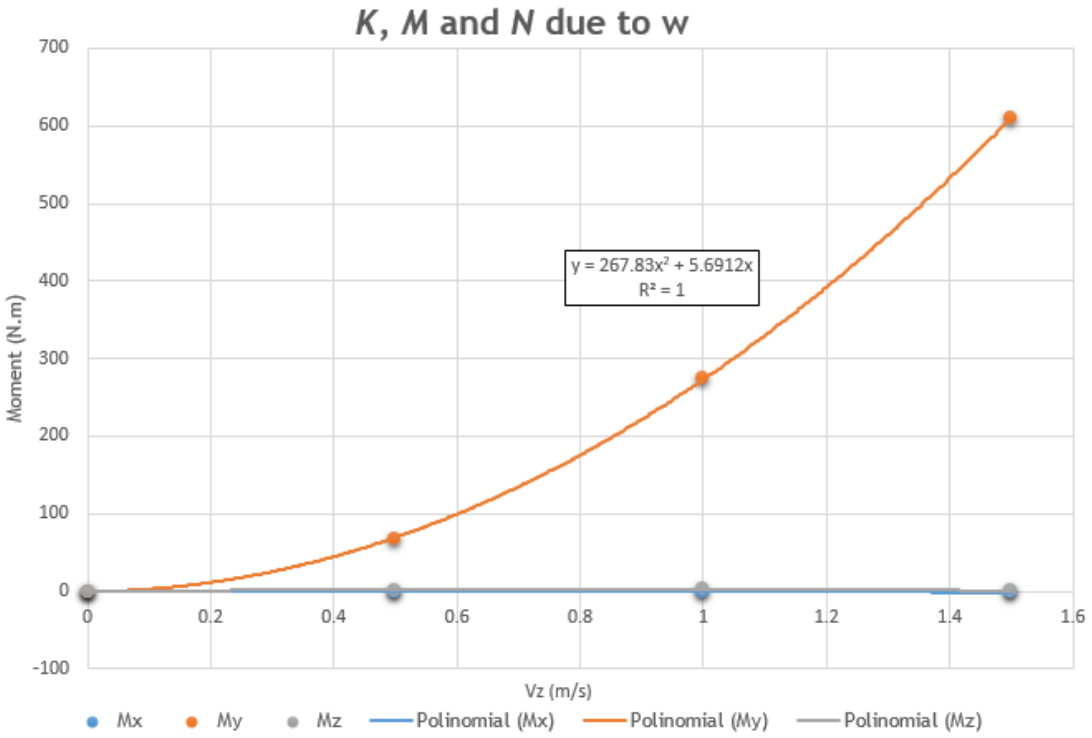

Figure 3.15: Static damping moments as a result of motion in heave.

In accordance with the hydrodynamic forces in surge and sway, motion in heave mostly induces damping forces within the same DoF.

Regarding the pitching moment, these coefficients were not expected since the horizontal fairings should induce a corrective moment, however, CFD data shows that the fairing contribution is not enough to correct the destabilizing contribution of the remaining components, however, this is corrected by the rotational damping due to pitch i.e. M_q and $M_{q|q|}$ (see section 3.2.5.3), and by the righting moment.

The coefficients for motion in heave are summarized below.

Table 3.15: Linear damping coefficients for motion in heave.

$X_w = 0.00$
$Y_w = 0.00$
$Z_w = 57.65$
$K_w = 0.00$
$M_w = 5.69$
$N_w = 0.00$

Table 3.16: Quadratic damping coefficients for motion in heave.

$X_{w\|w\|} = 0.00$
$Y_{w\|w\|} = 0.00$
$Z_{w\|w\|} = -606.06$
$K_{w\|w\|} = 0.00$
$M_{w\|w\|} = 267.83$
$N_{w\|w\|} = 0.00$

Note that quadratic curve fitting proves accurate since, for all fitting performed, the correlation coefficient (R-square) is ≈ 1.

3.2.5.3 Damping due to rotation

Following the previous discussion, the estimation of damping coefficients present a complex task. CFD analysis allowed for the estimation of parameters that arise from linear motion. However, and although estimation of rotational coefficients seems possible using CFD, these were not performed. Nevertheless, a common practice when modeling underwater vehicles, is to underestimate the damping force. This assures that the controller actuation is conservative, since a small force of resistance is expected. Complementary, if damping forces are overestimated, the controller might overcompensate since a greater amount of resistance is expected, leading to abnormal control [16].

In this context, it is possible to use data from other vehicles as long as it can be proven that damping forces for the latter are smaller. Since no data from similar vehicles is available, these were performed using a torpedo shaped AUV: the *Autolycus*. The Autolycus [30] is a lightweight torpedo shaped AUV. The very small size, when compared to the vehicle being developed at CEiiA (length = 1.4m, diameter = 0.12m) and the slender body type, suggests that damping should be smaller (this was confirmed by comparing the damping parameters determined for this AUV with the corresponding parameters for the Autolycus). According to Fossen [9], it is common to assume a diagonal structure of $\boldsymbol{D}$, therefore, only the hydrodynamic forces and moments that arise from rotational motion and, that are present in the diagonal structure of $\boldsymbol{D}$, are considered. Also, only the quadratic coeficients were considered for the Autolycus. According to Tang, 1999 [30]:

$$
\begin{aligned}
K_{p|p|} &\approx 0.0 \\
M_{q|q|} &= -18.0 \\
N_{r|r|} &= -17.8
\end{aligned}
$$

3.2.5.4 Hydrodynamic Forces Matrix

Introducing the damping coefficients of this vehicle to equation 1.33 and 1.34 yields:

$$
\boldsymbol{D}_l = \begin{bmatrix}
-7.66 & 0 & 0 & 0 & 0 & 0 \\
0 & -79.01 & 0 & 0 & 0 & 0 \\
3.53 & 0 & 57.65 & 0 & 0 & 0 \\
0 & -1.94 & 0 & 0 & 0 & 0 \\
0 & 44.82 & 5.69 & 0 & 0 & 0 \\
0 & -25.83 & 0 & 0 & 0 & 0
\end{bmatrix} \tag{3.19}
$$

$$\boldsymbol{D}_q(\boldsymbol{\nu}) = \begin{bmatrix} -29.05 \mid u \mid & 0 & 0 & 0 & 0 & 0 \\ 0 & -1506.5 \mid v \mid & 0 & 0 & 0 & 0 \\ -4.5 \mid u \mid & 0 & -606.06 \mid w \mid & 0 & 0 & 0 \\ 0 & -167.2 \mid v \mid & 0 & 0 & 0 & 0 \\ 0 & 24.28 \mid v \mid & 267.83 \mid w \mid & 0 & -18 \mid q \mid & 0 \\ 0 & -199.51 \mid v \mid & 0 & 0 & 0 & -17.8 \mid r \mid \end{bmatrix} \tag{3.20}$$

This results challenge the assumption regarding the damping forces matrices for the lateral subsystem in chapter 2. However, since damping is promotional to the velocity and lateral velocity is expected to remain very small, the pitch moment due to a lateral velocity is neglected.

3.2.6 Thrust

The propulsive force of the vehicle is provided by trolling motors. For the purpose of this thesis, the dynamics of the thrusters is neglected. However, the following restriction was provided by CEiiA:

- Maximum forward static thrust per motor: 117 Newton
- Maximum backward static thrust per motor: 95 Newton

Motor dynamics should be taken in consideration for the design of the control system.

The vector location, in relation to the CG, to the center of the propeller (assumed to be the point of action of the thrust) of each thruster was also determined using the 3D CAD model (in meters):

- Right longitudinal thruster

$$\mathbf{r}_{T1}^{g} = \begin{bmatrix} -0.689 & 0.300 & 0 \end{bmatrix}$$

- Left longitudinal thruster

$$\mathbf{r}_{T2}^{g} = \begin{bmatrix} -0.689 & -0.300 & 0 \end{bmatrix}$$

- Forward vertical thruster

$$\mathbf{r}_{T3}^{g} = \begin{bmatrix} 0.910 & 0 & 0.326 \end{bmatrix}$$

- Aft vertical thruster

$$\mathbf{r}_{T4}^{g} = \begin{bmatrix} -0.910 & 0 & -0.549 \end{bmatrix}$$

The vehicle is designed so that the vertical position of the longitudinal thrusters can be adjusted. In this context, the longitudinal thrusters are assumed to be horizontally aligned with the CG.

The force vector $\boldsymbol{U}$ can be expressed as:

$$\boldsymbol{U} = \begin{bmatrix} U_1 & U_2 & U_3 & U_4 & 0 & 0 \end{bmatrix}^T$$

Where U_1 is the thrust force applied by motor 1 and so on. According to the discussion in section 1.6.2.5, the mapping matrix relates the effects of each motor's thrust to the resulting force and/or moment. For this vehicle, the following mapping matrix is devised.

$$\boldsymbol{L} = \begin{bmatrix} 1 & 1 & 0 & 0 & 0 & 0 \\ 0 & 0 & 0 & 0 & 0 & 0 \\ 0 & 0 & 1 & 1 & 0 & 0 \\ 0 & 0 & 0 & 0 & 0 & 0 \\ 0) & 0 & \mathbf{r}_{T3}^{g}(1) & \mathbf{r}_{T4}^{g}(1) & 0 & 0 \\ \mathbf{r}_{T1}^{g}(2) & \mathbf{r}_{T2}^{g}(2) & 0 & 0 & 0 & 0 \end{bmatrix} \quad (3.21)$$

The thrust matrix for this vehicle is therefore expressed as:

$$\tau = \begin{bmatrix} 1 & 1 & 0 & 0 & 0 & 0 \\ 0 & 0 & 0 & 0 & 0 & 0 \\ 0 & 0 & 1 & 1 & 0 & 0 \\ 0 & 0 & 0 & 0 & 0 & 0 \\ 0 & 0 & 0.910 & -0.910 & 0 & 0 \\ 0.300 & -0.300 & 0 & 0 & 0 & 0 \end{bmatrix} \begin{bmatrix} U_1 \\ U_2 \\ U_3 \\ U_4 \\ 0 \\ 0 \end{bmatrix} \quad (3.22)$$

The force vector U is the only mean of motion control for the AUV, thus refereed to as the control vector.

An analysis of the mapping matrix shows that the roll and sway DoF do not present control thus, this vehicle is said to be underactuated, which means that active control is not present for all DoF. However, the hydrostatic matrix expressed in section 3.2.3 suggests that both roll and pitch are passively controlled. Although the sway DoF do not present passive nor active control, motion in yaw allows for complete freedom of movement. Also, in the context of a typical AUV mission (see section 1.3.1), lateral motion is not a requirement.

3.3 Limitations

The methods used to estimate parameters may induce two limitations: 1) the method used to estimate hydrodynamic coefficients is only valid for a small interval of angles of attack and side-slip, 2) parameters such as added mass and inertia are underestimated. Such limitations should be assessed in the context of control.

Although the envelope of angles of attack and side-slip is restricted, the same do not compromise the use of the vehicle in the scope of proposed mission scenarios.

In most cases, if there is uncertainty regarding a given parameter value, it is always better to either underestimate or overestimate. For a second order system, two major properties are in the interest of control: the natural frequency and damping ratio. An example of such systems is the characteristic decoupled equation of motion for pitch which can be found in [9]:

$$(I_y - M_{\dot{q}})\ddot{\theta} - M_q\dot{\theta} + Wz_b\theta = \tau_5 \quad (3.23)$$

According to the discussion in section 3.2.5.3, it is more advantageous to underestimate damping parameters since it leads to conservative control.

Regarding the natural frequency, a high value is always problematic since the controller (and actuator) has less time to act. Thus, overestimating the natural frequency is a more conservative approach. The characteristic natural frequency for pitch is expressed as:

$$\omega_{pitch} = \sqrt{\frac{W z_b}{I_y - M_{\dot{q}}}} \quad (3.24)$$

This shows that the natural frequency is inversely proportional to the inertia and added mass (I_y and $M_{\dot{q}}$, respectively) thus, in order to overestimate the natural frequency, the inertia and added mass should be underestimated. This holds truthful for roll. Since the inertia and added mass were underestimated (see sections 3.2.2 and 3.2.4), although controller performance might suffer, abnormal control is avoided. It is imperative that, for motion other than pitch and roll, the consequences of underestimation shall be addressed in the future.

Chapter 4

Simulation

This chapter addresses the validation of the longitudinal and lateral subsystems by comparing simulation results with the complete model. 6DoF motion simulation for the AUV being developed at CEiiA are also performed and analyzed. Four individual simulation programs were written in *MATLAB*[1] with help of the Marine Systems Simulator (MSS) toolbox[2]:

- *6DoF using quaternions.*
- *6DoF using euler angles.*
- *Longitudinal subsystem.*
- *Lateral subsystem.*

Results for quaternions and euler angle proved identical thus, quaternions were used for the following simulations.

The simulation were developed in the following manner:

Begin
Introduce initial position and states
Introduce simulation time interval and step
    For: time interval
        Thrust vector $\boldsymbol{U}$ for i step
        Calculate system's matrices ($\dot{\boldsymbol{\nu}}$ and $\dot{\boldsymbol{\eta}}$)
        Run numeric integration
        Save data
    End For
Plot data
End

[1] MATLAB R2015a, The MathWorks Inc.
[2] Copyright (C) 2008 Thor I. Fossen and Tristan Perez. Downloaded under General Public License.

4.1 Remarks on the Following Simulations

One of the problems encountered, while performing the simulations, was the destabilizing effect of the Coriolis. Since nonlinear feedback controllers are capable of dominating such forces [16], the Coriolis forces are not hereby considered. All following simulations were performed assuming depth control i.e. $B = W$. To improve visualization, the *down* coordinate was inverted. Simulation step is 0.01 seconds.

4.2 Validation of the 3DoF Subsystems

Since the 3DoF subsystems were devised by the author, validation is required. Little interaction is expected between both subsystems therefore, for control inputs that do not induce interaction between the two subsystems, the value of the state variable of the subsystem and the corresponding state variables of complete model should present similar values. Thus, the following validation test was devised:

1. Run a decoupled maneuver for the corresponding subsystem.

2. Run the same maneuver for the 6DoF model.

3. Compare results.

If results are similar, the subsystem is considered valid.

A typical test for floating vessels is the *zig-zag* maneuver [59]. Since this maneuver addresses motion in the lateral plane, it is used to assess the validity of the lateral subsystem. For the longitudinal subsystem, the *dive and ascent* maneuver is used.

4.2.1 Longitudinal Validity Test - Dive and Ascent Maneuver

The dive and ascent maneuver is performed by administering different force values for the vertical thrusters for a given time interval. A force of 15 Newton is also administered to each horizontal thruster to provide forward velocity (total forward thrust: 30N). Force values for the vertical thrusters are expressed in the following table:

Table 4.1: Vertical thrust for the dive and ascent maneuver.

Time interval [s]	Forward thruster [N]	Aft thruster [N]
0 to 10	-40	-40
10 to 30	40	40
30 to 50	-40	-40
50 to 70	40	40
70 to 80	-40	-40

Simulation time is 80 seconds. Initial states and position are zero.

- Results for the longitudinal subsystems

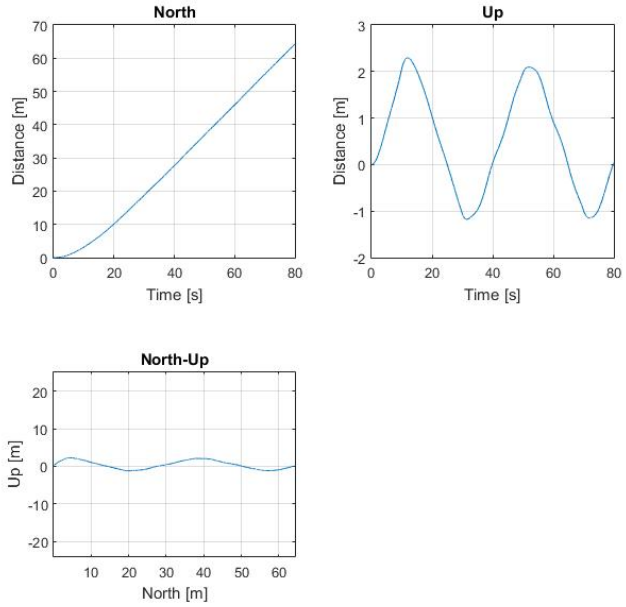

Figure 4.1: Longitudinal subsystem trajectory for the dive and ascent maneuver (80s simulation).

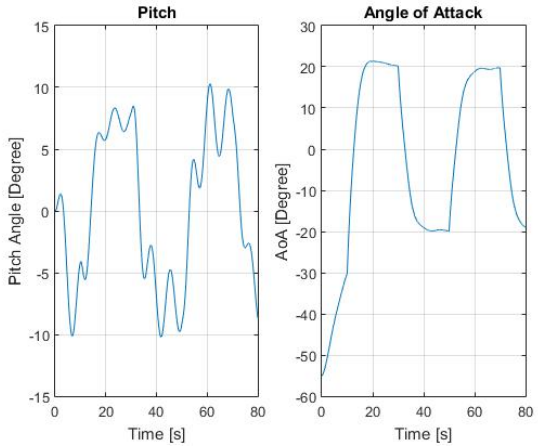

Figure 4.2: Longitudinal subsystem AoA and pitch angle for the dive and ascent maneuver (80s simulation).

- Results for the complete model

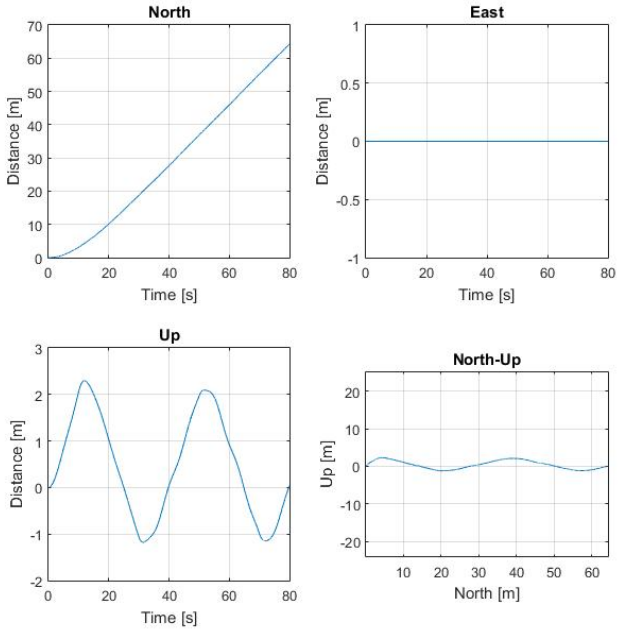

Figure 4.3: Complete model trajectory for the dive and ascent maneuver (80s simulation).

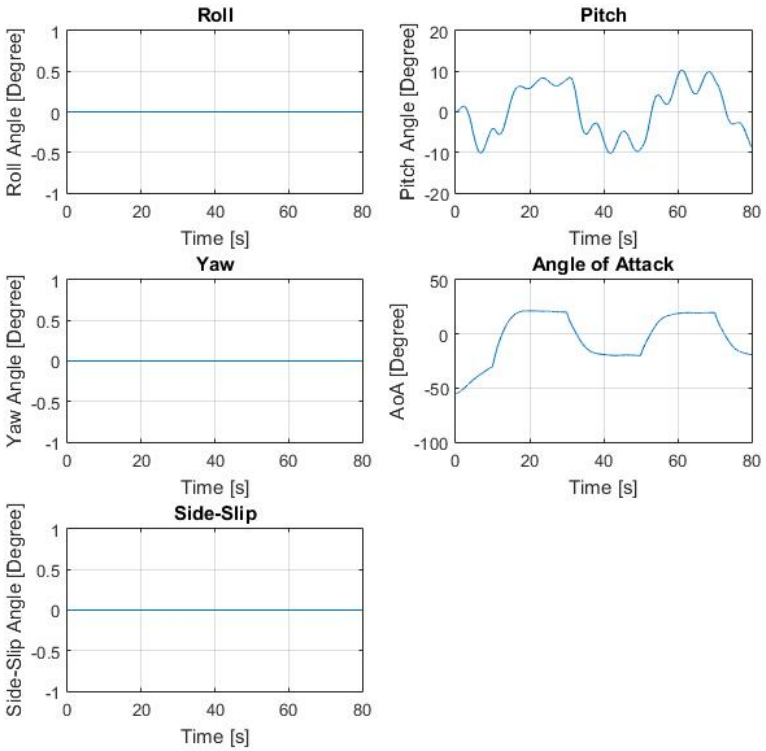

Figure 4.4: Complete model AoA and pitch angle for the dive and ascent maneuver (80s simulation).

Analysis of the Results - Dive and Ascent Maneuver: The results obtain using both models were identical. As expected, the vehicle ascends for negative values of thrust and dives for the positive ones (see figures 4.1 and 4.3). Figure 4.4 also suggests that the lateral subsystem is not influenced since since roll, yaw and side-slip stayed constant. This analysis validates the assumptions and simplifications performed for the longitudinal model. Note that although $\alpha < -25°$ for the first 10 seconds, however, this does not compromise validation since the purpose is comparing results. The velocity data for this simulations can be found in appendix A.

4.2.2 Lateral Validity Test - Zig-Zag Maneuver

The zig-zag maneuver was performed by administering different force values to the left and right thrusters. This induces a moment in yaw, as discussed in section 3.2.6. Force parameters, for the horizontal thrusters, is expressed in the following table:

Table 4.2: Motor thrust for zig-zag maneuver.

Time interval [s]	Right thruster [N]	Left thruster [N]
0 to 10	10	20
10 to 30	20	10
30 to 50	10	20
50 to 70	20	10
70 to 80	10	20

Since a constant surge velocity (u_k) is assumed for the lateral subsystem (see section 2.2), it is necessary to determine surge velocity for this maneuver given the thrust parameters mentioned above. For the effect, the complete model was simulated for this maneuver starting with zero velocity.

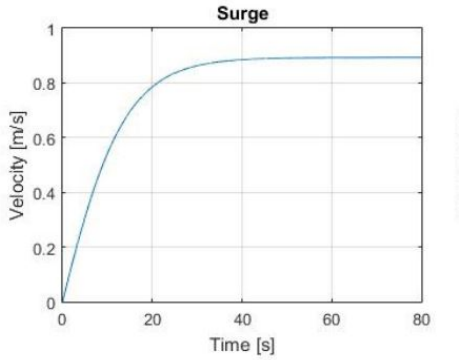

Figure 4.5: Terminal velocity for the zig-zag maneuver.

Figure 4.5 suggests that terminal velocity is approximately 0.9 m/s. Therefore, $u_k = 0.9$ for the lateral subsystem and $u_0 = 0.9$ (initial surge velocity) for the complete model. Time for the following simulations is 80 seconds. Initial states and position are zero except for surge velocity.

- Results for the lateral subsystem

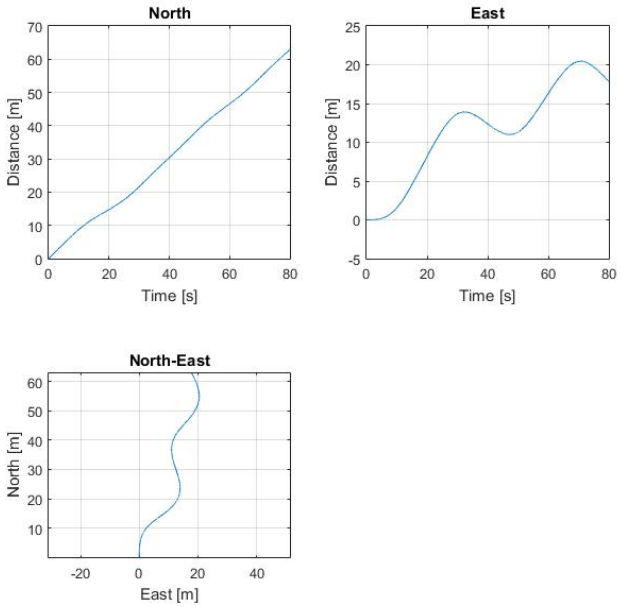

Figure 4.6: Lateral subsystem trajectory for the zig-zag maneuver (80s simulation).

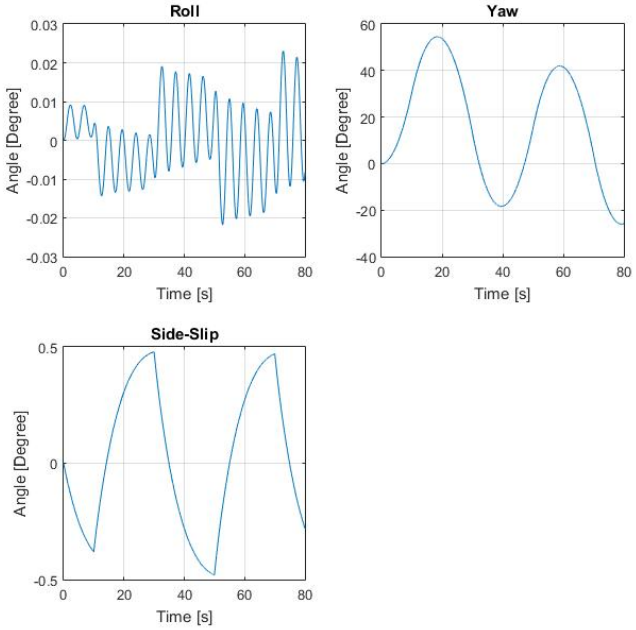

Figure 4.7: Lateral subsystem side-slip, yaw and roll angles for the zig-zag maneuver (80s simulation).

- Results for the complete model

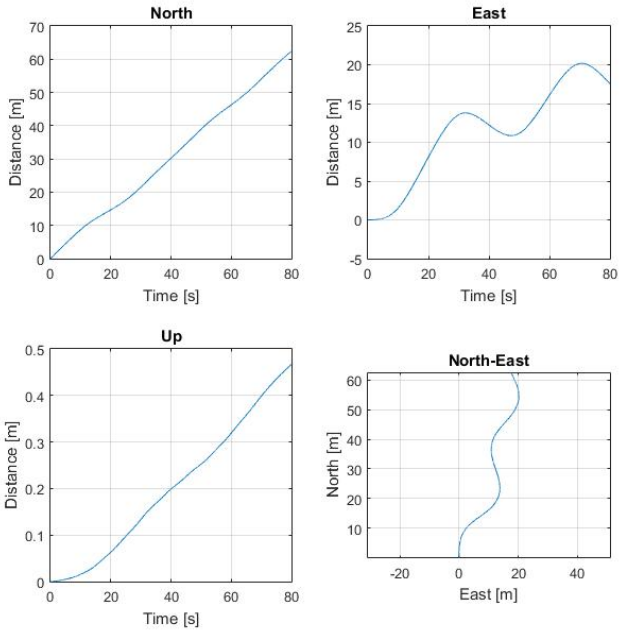

Figure 4.8: Complete model trajectory for the zig-zag maneuver (80s simulation).

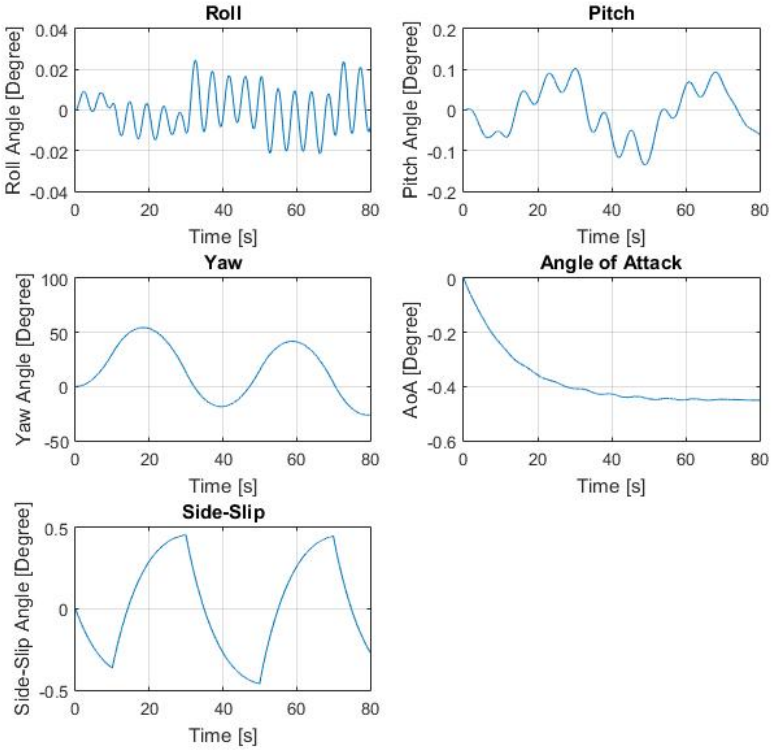

Figure 4.9: Complete model attitude, AoA and side-slip angles for the zig-zag maneuver (80s simulation).

Analysis of the Results - Zig-Zag Maneuver: The trajectories using both models are very similar (see figures 4.7 and 4.9). However, a comparison between figure 4.7 and figure 4.9 suggests the roll DoF presents slight variations. It is also noticeable that motion in the lateral subsystem induced small disturbances to the longitudinal subsystem (see figure 4.9). This is probably due to the pitching moment created by a a lateral velocity (see section 3.2.5.2). Yet, this moment is small when compared to the overall forces acting of the vehicle. Therefore, it can be easily dominated by applying control to the longitudinal subsystem. Since control of the longitudinal subsystem is a consideration for devising the lateral subsystem. This validates the lateral subsystem. Again, the velocity data for this simulations can be found in appendix A.

4.3 Helical Diving Test

The helical diving test is intended at analyzing the response of the vehicle to coupled motion scenarios. A simple helical diving test was devised using the following values of force, for each thruster, during the entire simulation (80 seconds): The force difference between the left and

Table 4.3: Motor thrust for the helical diving test.

Right thruster [N]	Left thruster [N]	Forward thruster [N]	Aft thruster [N]
5	10	2	1

right thrusters is expected to create a positive yaw moment. The horizontal thrusters are also expected to provide forward velocity. Analogously,the vertical thrusters are expected to induce a negative pitch moment (nose down attitude) and a positive heave velocity (down). Initial states and position are all zero.

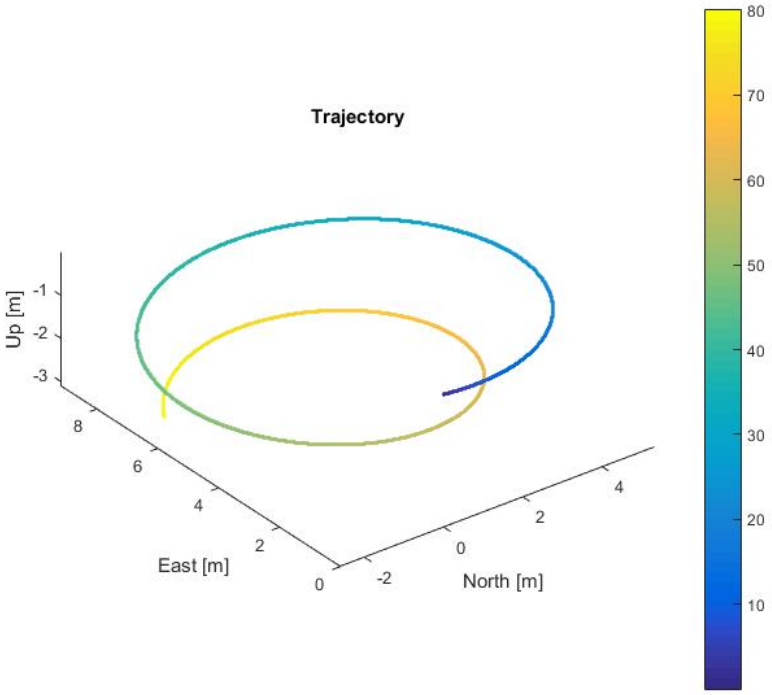

Figure 4.10: Helical diving test trajectory (Color bar indicates time - 80s).

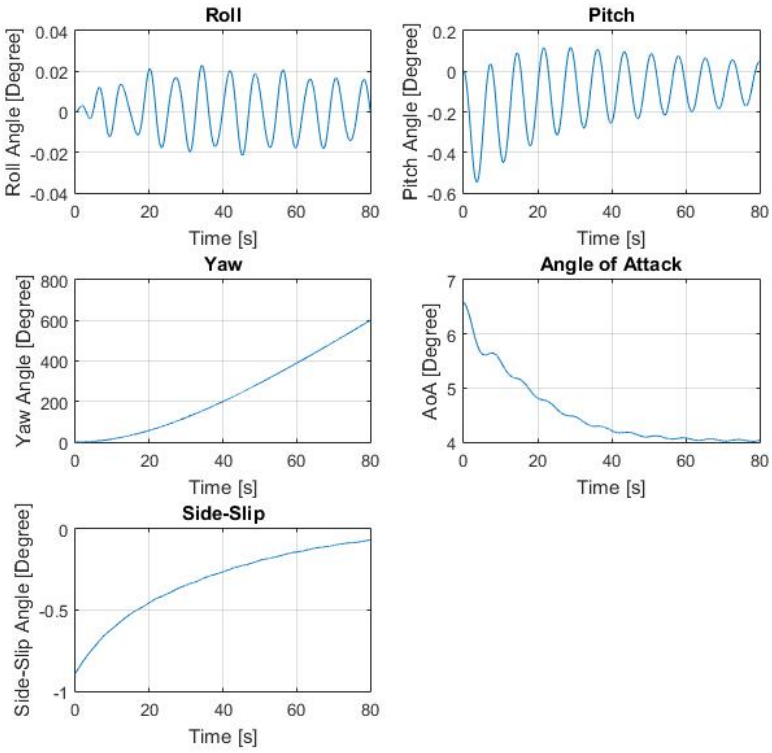

Figure 4.11: Helical diving test attitude, AoA and side-slip angle (80s simulation).

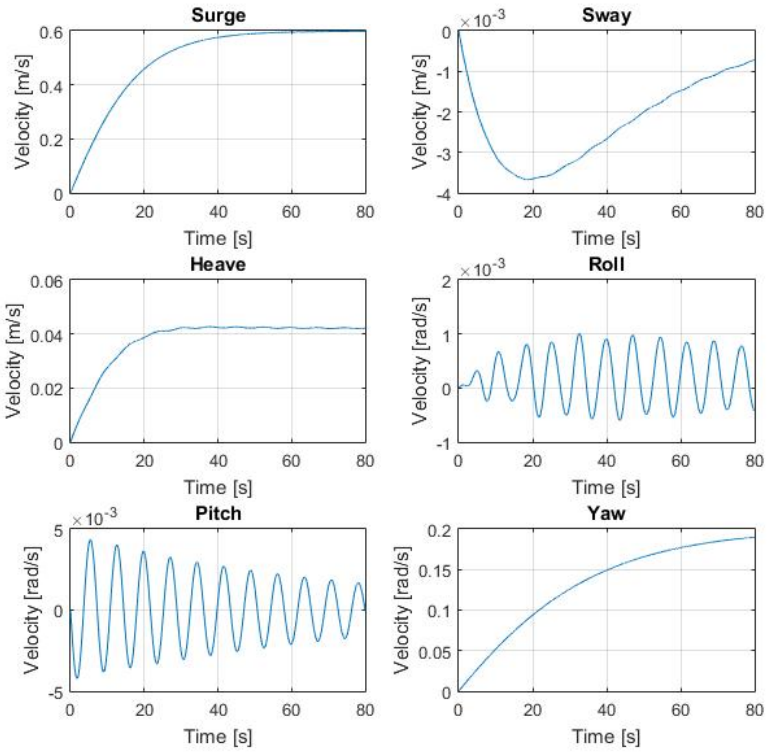

Figure 4.12: Helical diving test linear and angular velocities (80s simulation).

As expected, the resulting trajectory is a downward spiral. According to figure 4.12, the vehicle accelerates in surge and heave but lateral velocity is negligible. Also, since the lateral velocity is small and, following the discussion in section 3.2.5.2, the destabilizing yaw moment induced by a lateral velocity is also negligible. Moreover, the stabilizing effect of yaw damping due to rotation, is present since yaw velocity > 0. Small roll angles are also expected due to the correcting effect of the righting moment. Although a nose down attitude was expected, figure 4.11 suggests that the pitch angle stabilizes at approximately zero degrees. This is probably due to the destabilizing effect of heave in pitch (see section 3.2.5.2). An analysis of the dive and ascent maneuver also reinforces this hypothesis. Figures 4.8 and 4.8 show that when the vehicle is ascending, the pitch angle is negative (nose down) and, when diving, the pitch angle is positive (nose up). This is very inefficient since it leads to high angles of attack thus increasing drag.

Chapter 5

Conclusions

The dynamics of underwater vehicle are complex. Plenty of research exists on the dynamics of torpedo shaped AUVs, however, since multi-body AUVs are scarce (only two double body platforms where the bodies are vertically align were found), knowledge of the dynamic characteristics for these vehicles is limited. The research developed in modeling the AUV expands on this knowledge.

5.1 Conclusions on the Dynamic Models

For slender body vehicles, a common modeling approach is to decouple the lateral and longitudinal motions since it provides a simpler approach to control. Since the AUV is, essentially, the combination of two torpedo shaped bodies, this suggests that the lateral and longitudinal subsystems can be decoupled for this vehicle. This decomposition proves valid if the damping matrices can be expressed in the following form:

$$\boldsymbol{D} = \begin{bmatrix} d_{11} & 0 & d_{13} & 0 & d_{15} & 0 \\ 0 & d_{22} & 0 & d_{24} & 0 & d_{26} \\ d_{31} & 0 & d_{33} & 0 & d_{35} & 0 \\ 0 & d_{42} & 0 & d_{44} & 0 & d_{46} \\ d_{51} & 0 & d_{53} & 0 & d_{55} & 0 \\ 0 & d_{62} & 0 & d_{64} & 0 & d_{66} \end{bmatrix}$$

Although this is not the case for this vehicle, the validation tests performed in sections 4.2 and 4.2.1 suggests that a) the longitudinal subsystem is not affected b) influence to the lateral subsystem is small and controllable.

Note that although simplifications were performed, namely $\mathbf{r}_g^b = \mathbf{0}_{3\times 1}$ and vertical alignment of the CB and CG, these can be adopted for most AUVs.

The research of this thesis suggests that decoupling the lateral and longitudinal subsystems is valid for double body AUV where both bodies are vertically aligned. Since, for the design of the control systems, it is advantageous to simplify the models, the 3DoF subsystems might prove advantageous [60].

5.2 Conclusions of the Parameter Estimation

The estimation of parameters using computational and analytical methods proved time-efficient and low cost. The estimation of hydrodynamic coefficients due to heave and sway by extrapolating CFD data at various velocities and angles of attack and side-slip proves advantageous (when compared to the traditional analytic and experimental methods) since it avoids lengthy calculations and/or tests. Watt's method for estimating added mass also proved helpful since it allowed for fast estimation. However, since geometric simplifications had to be performed, results are probably underestimated. Although parameters such as inertia, added mass and rotational damping are underestimated, the discussion of section 3.3 shows that, even if controller performance is reduced, the dynamic models devised in this thesis are suitable for controller design. Also, since the methods used for estimating parameters are not specific for the AUV being developed at CEiiA, these methods can be adopted for various body-types.

5.3 Conclusions on the Dynamics of the AUV

Probably the most worrying dynamic dynamic characteristic of the AUV studied in this thesis, is that the hydrodynamic fairings fail to correct the overall destabilizing moment of the vehicle in yaw and pitch. Since the lateral velocity is expected to be small and the yaw DoF is actuated, the destabilizing effect of a lateral velocity is not problematic. However, since velocity in heave is expected to be much greater the resulting moment, for diving and ascending for example, may prove difficult to correct. It is important to note that the vertical thrusters are also responsible for counteracting the the residual buoyancy force, thus reducing the effective power available to control pitch. Attenuation of the destabilizing moment in pitch could be achieved by increasing the chord and span of the horizontal fairing and/or increasing distance between the the fairing and the center of gravity.

5.4 Future Work

Modeling the AUV being developed at CEiiA allowed better understanding of current capabilities and limitations. Although this works addresses the dynamic models for the design of control system, the areas of guidance and navigation are also of the utmost importance to achieve robust autonomous capabilities. The guidance and navigation systems should therefore be addressed and subsequently integrated with the control system.

5.4.1 Modeling

Research aimed at improving the dynamic models used throughout this thesis should focus on:

- Adapting the damping matrices to better model the damping forces.
- Including motor dynamics and ocean currents.
- Include the dive and ascent mission stages.

Better understanding of the destabilizing influence of the Coriolis forces shall also be addresses in future studies.

5.4.2 Dynamic Parameters

Since computational methods are time-efficient and low cost, it makes sense to further develop this capability to better model dynamic parameters, particularly for the estimation of hydrodynamic parameters.

In the context of validating or improving estimations, the following procedure is recommended:

1. Confirm the estimated dry mass by weighing the vehicle. If estimation proves incorrect, revisit the mass matrix.
2. Check the buoyancy force by tests in a water tank. Readdress the hydrostatic forces vector if necessary.
3. Perform system identification to validate hydrodynamic damping and added mass. Adjust the respective matrices if necessary.

5.4.3 The AUV

Instabilities identified while modeling the hydrodynamic damping, require further study to assess a) their effect on vehicle performance b) the capability of the thrusters to correct them. Addressing this issue is crucial for the success of the control system and should be carried out before it is designed. Devising simulation tests aimed at evaluating performance and maneuvering capabilities may also prove valuable for detection of unforeseen issues.

Bibliography

[1] “Unmanned Submersibles (ROV, AUV) and Underwater Working Machines,” DNV GL, Norm I-5, 2009. 1, 5

[2] L. Brun, “ROV/AUV Trends: Market and Technology,” *Marine Technology Reporter*, Sep. 2012. 1, 2

[3] D. R. Blidberg, “The development of autonomous underwater vehicles (AUV); a brief summary,” in *IEEE ICRA*, vol. 4, 2001. 1, 2, 3, 4

[4] “The Navy Unmanned Undersea Vehicle (UUV) Master Plan,” Nov. 2004. 1, 2, 4

[5] R. B. Wynn, V. A. Huvenne, T. P. Le Bas, B. J. Murton, D. P. Connelly, B. J. Bett, H. A. Ruhl, K. J. Morris, J. Peakall, D. R. Parsons, E. J. Sumner, S. E. Darby, R. M. Dorrell, and J. E. Hunt, “Autonomous Underwater Vehicles (AUVs): Their past, present and future contributions to the advancement of marine geoscience,” *Marine Geology*, vol. 352, pp. 451–468, Jun. 2014. 1, 2

[6] D. Bingham, T. Drake, T. Hill, and R. Lott, “The Application of Autonomous Underwater Vehicle (AUV) Technology in the Oil Industry – Vision and Experiences,” Washington, D.C. USA, Apr. 2002. 1, 2, 4

[7] R. L. Wernli, “AUV commercialization-who’s leading the pack?” DTIC Document, Tech. Rep., 2000. [Online]. Available: http://oai.dtic.mil/oai/oai?verb=getRecord&metadataPrefix=html&identifier=ADA422192 2

[8] L. Paull, S. Saeedi, M. Seto, and H. Li, “AUV Navigation and Localization - A Review,” Defense R&D Canada, Canada, Tech. Rep., 2013. 3

[9] T. I. Fossen, *Handbook of marine craft hydrodynamics and motion control*. Wiley, 2011. 3, 14, 19, 20, 27, 29, 31, 61, 64

[10] “Curator’s Choice -Whitehead torpedo.” [Online]. Available: http://www.submarine-museum.co.uk/what-we-have/our-favourite-objects/whitehead-torpedo 3

[11] J. Edward and S. Roderick, *Submarine Torpedo Tactics: An American History*. North California: McFarland & Company, 2015. 3

[12] Stuart Bennett, “A brief history of automatic control,” *IEEE Control Systems Magazine*, vol. 16, no. 3, pp. 17–25, 1996. [Online]. Available: http://www.elai.upm.es/moodle/pluginfile.php/1792/mod_resource/content/0/articulos/HistoryOfControl.pdf 3, 4

[13] ——, *A history of control engineering 1930 - 1955*, ser. IEE control engineering series. London: Peregrinus, 1993, no. 47, oCLC: 636824364. 3, 4

[14] “Remotely Operated Vehicle Committee of the Marine Technology Society.” 3

[15] G. N. Roberts and R. Sutton, *Advances in unmanned marine vehicles*. Iet, 2006, vol. 69. 4

[16] J. E. G. Refsnes, “Nonlinear model-based control of slender body AUVs,” *Norwegian University of Science and Technology*, vol. 30, no. 226, pp. 229–231, 2007. 4, 27, 55, 61, 68

[17] H. R. Widditsch, “SPURV-The first decade,” DTIC Document, Tech. Rep., 1973. 4

[18] G. Griffiths and I. Edwards, “AUVs: designing and operating next generation vehicles,” in *Elsevier Oceanography Series*. Elsevier, 2003, vol. 69, pp. 229–236. 4

[19] “robot | technology | Britannica.com.” [Online]. Available: https://www.britannica.com/technology/robot-technology 4

[20] “AUVAC: Strengthening the AUV Community.” [Online]. Available: http://auvac.org/ 4

[21] C. Roman, O. Pizarro, R. Eustice, and H. Singh, “A new autonomous underwater vehicle for imaging research,” vol. 1. IEEE, 2000, pp. 153–156. [Online]. Available: http://ieeexplore.ieee.org/lpdocs/epic03/wrapper.htm?arnumber=881251 5

[22] “SeaBED :: Hanumant Singh Lab.” [Online]. Available: http://web.whoi.edu/singh/auvasf/seabed/ 8

[23] D. Shea, C. Williams, M. He, P. Crocker, N. Riggs, and R. Bachmayer, “Design and testing of the Marport SQX-500 twin-pod AUV,” in *IEEE AUV 2010 Conference proceedings*, 2010. [Online]. Available: http://nparc.cisti-icist.nrc-cnrc.gc.ca/npsi/ctrl?action=rtdoc&an=17670185 8

[24] SNAME, “The Society of Naval Architects and Marine Engineers. Nomenclature for Treating the Motion of a Submerged Body Through a Fluid,” Tech. Rep., 1950. 9, 23, 25

[25] T. I. Fossen, *Guidance and Control of Ocean Vehicles*. University of Trondheim, Norway: Wiley, 1994. 9, 30

[26] D. Rowell, “State-space representation of lti systems,” *URL: http://web. mit. edu/2.14/www/Handouts/StateSpace. pdf*, 2002. [Online]. Available: http://www.academia.edu/download/39702214/StateSpace_ecuations.pdf 11

[27] M. Gertler and G. R. Hagen, “Standard equations of motion for submarine simulation,” DTIC Document, Tech. Rep., 1967. [Online]. Available: http://oai.dtic.mil/oai/oai?verb=getRecord&metadataPrefix=html&identifier=AD0653861 11

[28] J. Feldman, “DTNSRDC Revised Standard Submarine Equations of Motion,” David Taylor Naval R&D Center, Tech. Rep. DTNSRDC/SPD -0393-09., 1979. 11

[29] H. Aschemann, *New approaches in automation and robotics*. Vienna, Austria: I-Tech Education and Publishing, 2008, oCLC: 908264619. 11, 12

[30] S. C. Tang, "Modeling and simulation of the autonomous underwater vehicle, Autolycus," Ph.D. dissertation, Massachusetts Institute of Technology, 1999. [Online]. Available: http://dspace.mit.edu/handle/1721.1/80002 12, 50, 61

[31] D. E. Humphreys, "Development of the Equations of Motion and Transfer Functions for Underwater Vehicles." DTIC Document, Tech. Rep., 1976. [Online]. Available: http://oai.dtic.mil/oai/oai?verb=getRecord&metadataPrefix=html&identifier=ADA033882 12

[32] M. Nahon, "A simplified dynamics model for autonomous underwater vehicles," in *Autonomous Underwater Vehicle Technology, 1996. AUV'96., Proceedings of the 1996 Symposium on*. IEEE, 1996, pp. 373–379. [Online]. Available: http://ieeexplore.ieee.org/xpls/abs_all.jsp?arnumber=532437 12

[33] T. I. Fossen, "Nonlinear Modelling and Control of Underwater Vehicles," PhD, Norwegian Institute of Technology, 1991. 12, 13, 20

[34] B. Etkin and L. D. Reid, *Dynamics of flight: stability and control*, 3rd ed. New York: Wiley, 1996, oCLC: 832681625. 15

[35] O.-E. Fjellstad and T. I. Fossen, "Quaternion feedback regulation of underwater vehicles," in *3rd IEEE Conference on Control Application*, 1994, pp. 24–26. [Online]. Available: https://www.researchgate.net/profile/Thor_Fossen/publication/3598366_Quaternion_feedback_regulation_of_underwater_vehicles/links/0deec517a98329cfbf000000.pdf 16, 20

[36] J. v. Oosten, "Understanding Quaternions," Jun. 2012. [Online]. Available: http://www.3dgep.com/understanding-quaternions/ 16

[37] O.-E. Fjellstad and T. I. Fossen, "Position and attitude tracking of AUV's: a quaternion feedback approach," *IEEE Journal of Oceanic Engineering*, vol. 19, no. 4, pp. 512–518, 1994. [Online]. Available: http://ieeexplore.ieee.org/xpls/abs_all.jsp?arnumber=338387 16

[38] J. B. Kuipers, *Quaternions and Rotation Sequence*. Princeton University Press, 1999. 16

[39] D. R. Wilkins, "William Rowan Hamilton: mathematical genius," *Physics World*, Aug. 2005. 16

[40] F. P. Beer, Ed., *Vector mechanics for engineers. Statics and dynamics*, 9th ed. Boston: McGraw-Hill Companies, 2010. 19, 45

[41] A. B. Biran, *Ship hydrostatics and stability*, repr ed. Amsterdam: Butterworth-Heinemann, 2007, oCLC: 254900025. 21

[42] F. H. Imlay, “The complete expressions for added mass of a rigid body moving in an ideal fluid,” DTIC Document, Tech. Rep., 1961. [Online]. Available: http://oai.dtic.mil/oai/oai?verb=getRecord&metadataPrefix=html&identifier=AD0263966 22

[43] G. D. Watt, “Estimates for the Added Mass of a Multi-Component, Deeply Submerged Vehicle.” DTIC Document, Tech. Rep., 1988. [Online]. Available: http://oai.dtic.mil/oai/oai?verb=getRecord&metadataPrefix=html&identifier=ADA203234 23, 50, 52, 53

[44] S. Lihua, “Calculation of Added Mass for Underwater Vehicles Based on FVM,” 2016. [Online]. Available: http://www.atlantis-press.com/php/download_paper.php?id=25854773 23

[45] G. Conte, S. M. Zanoli, D. Scaradozzi, and A. Conti, “Evaluation of hydrodynamics parameters of a UUV. A preliminary study,” in *Control, Communications and Signal Processing, 2004. First International Symposium on*. IEEE, 2004, pp. 545–548. [Online]. Available: http://ieeexplore.ieee.org/xpls/abs_all.jsp?arnumber=1296437 25, 44, 54

[46] S. Tang, T. Ura, T. Nakatani, B. Thornton, and T. Jiang, “Estimation of the hydrodynamic coefficients of the complex-shaped autonomous underwater vehicle TUNA-SAND,” *Journal of Marine Science and Technology*, vol. 14, no. 3, pp. 373–386, Sep. 2009. [Online]. Available: http://link.springer.com/10.1007/s00773-009-0055-4 25

[47] M. J. Griffin, “Numerical prediction of the maneuvering characteristics of submarines operating near the free surface,” Ph.D. dissertation, Massachusetts Institute of Technology, 2002. [Online]. Available: http://dspace.mit.edu/handle/1721.1/8327 25

[48] J. Vervoort, *Modeling and control of an unmanned underwater vehicle*. Christchurch: University of Canterbury, 2009. [Online]. Available: http://www.mate.tue.nl/mate/pdfs/10894.pdf 26

[49] B. Ferreira, A. Matos, N. Cruz, and M. Pinto, “Modeling and Control of the MARES Autonomous Underwater Vehicle,” *Marine Technology Society Journal*, vol. 44, no. 2, p. 19. 26

[50] J.-J. E. Slotine and W. Li, *Applied nonlinear control*. Englewood Cliffs, NJ: Prentice Hall, 1991, oCLC: 21227927. 26

[51] K. M. Tan, A. Anvar, and T. F. Lu, “Autonomous underwater vehicle (AUV) dynamics modeling and performance evaluation,” in *Proceedings of World Academy of Science, Engineering and Technology*. World Academy of Science, Engineering and Technology, 2012. [Online]. Available: http://www.waset.org/publications/9586 27

[52] J. S. Geisbert, “Hydrodynamic modeling for autonomous underwater vehicles using computational and semi-empirical methods,” 2007. [Online]. Available: https://vtechworks.lib.vt.edu/handle/10919/33195 44

[53] T. Prestero, “Verification of a six-degree of freedom simulation model for the

REMUS autonomous underwater vehicle," Ph.D. dissertation, Massachusetts Institute of Technology and Woods Hole Oceanographic Institution, 2001. [Online]. Available: https://darchive.mblwhoilibrary.org/handle/1912/3040 44

[54] Z. Jinxin, S. Yumin, J. Lei, and C. Jian, "Hydrodynamic performance calculation and motion simulation of an AUV with appendages," in *Electronic and Mechanical Engineering and Information Technology (EMEIT), 2011 International Conference on*, vol. 2. IEEE, 2011, pp. 657–660. [Online]. Available: http://ieeexplore.ieee.org/xpls/abs_all.jsp?arnumber=6023135 44

[55] G. Indiveri, "Modelling and identification of underwater robotic systems," Ph.D. dissertation, 1998. [Online]. Available: ftp://transit-port.net/Publications/1998/Indiveri.PhD.98.pdf 44

[56] "Pressure hull and structures - Stability and buoyancy," DNV GL, Norm III-7, 2015. 48

[57] J. N. Newman, *Marine hydrodynamics*, 5th ed. Cambridge, Mass.: MIT Pess, 1986, oCLC: 258074446. 50, 54

[58] V. Berg, "Development and Commissioning of a DP system for ROV SF 30k," MSc, Norwegian University of Science and Technology, 2012. 54

[59] M. Triantafyllou and F. Hover, "Maneuvering and Control od Marine Vehicles," 2013. 68

[60] J. Petrich and D. J. Stilwell, "Model simplification for AUV pitch-axis control design," *Ocean Engineering*, vol. 37, no. 7, pp. 638–651, 2010. [Online]. Available: http://www.sciencedirect.com/science/article/pii/S0029801809002649 79

BIBLIOGRAPHY

Appendix A

Simulation Graphics

A.1 Validation Tests

A.1.1 Zig-Zag Maneuver

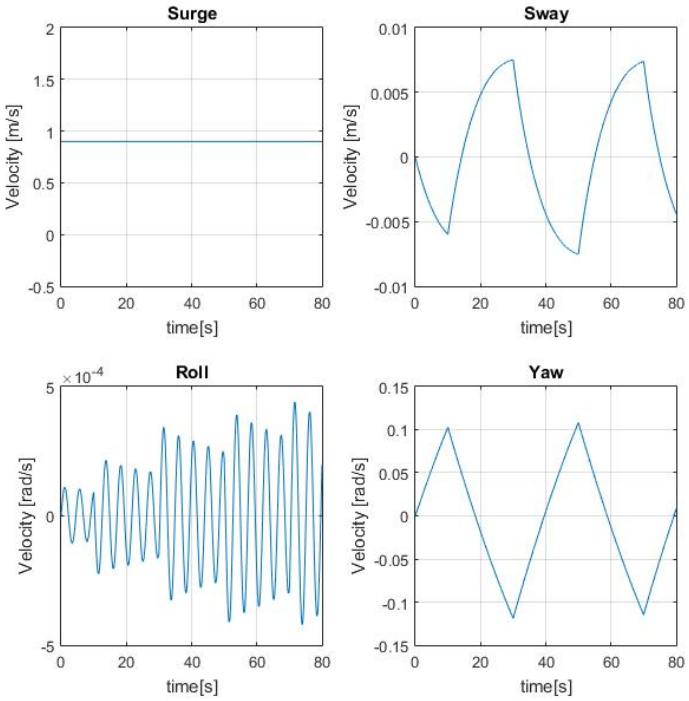

Figure A.1: Lateral subsystem velocities for the zig-zag maneuver (80s simulation).

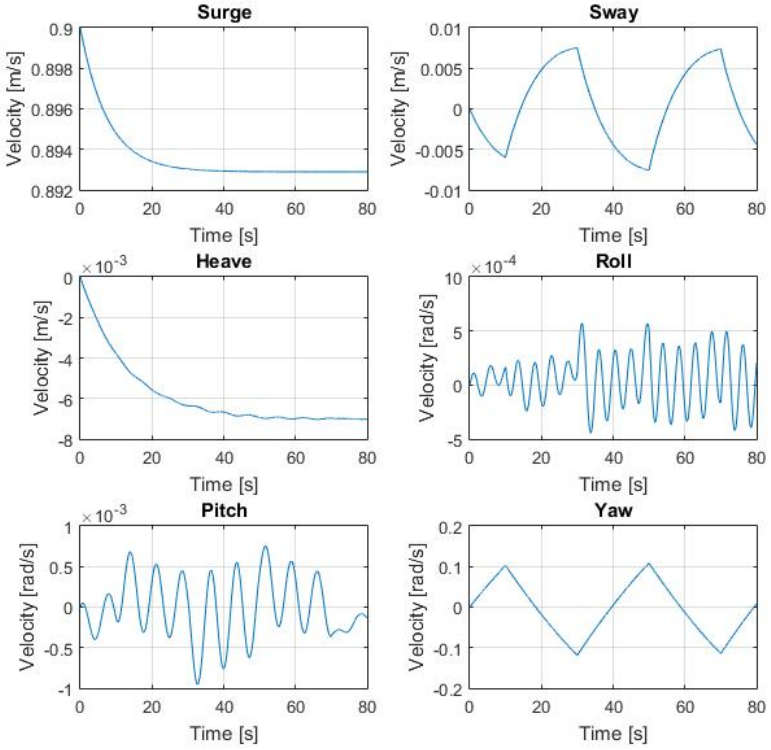

Figure A.2: Complete model velocities for the zig-zag maneuver (80s simulation).

A.1.2 Dive and Ascent Maneuver

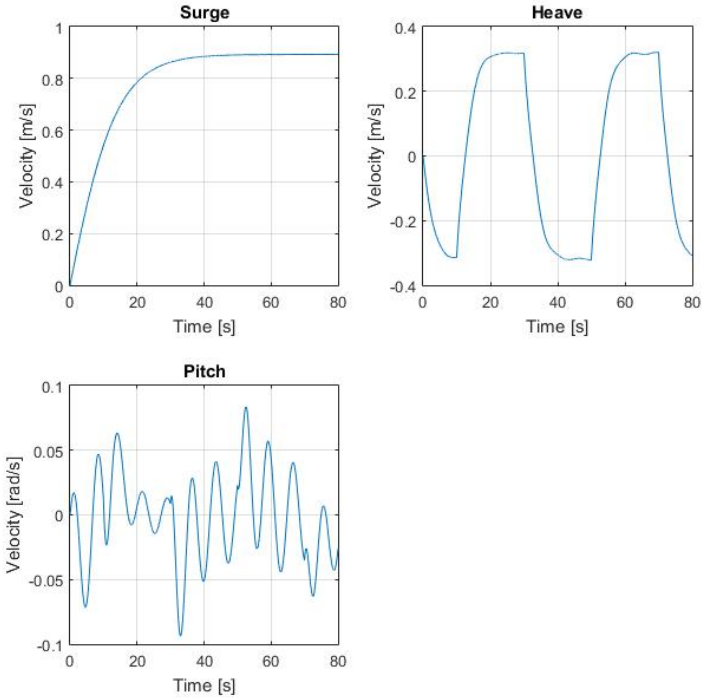

Figure A.3: Longitudinal subsystem velocities for the dive and ascent maneuver (80s simulation).

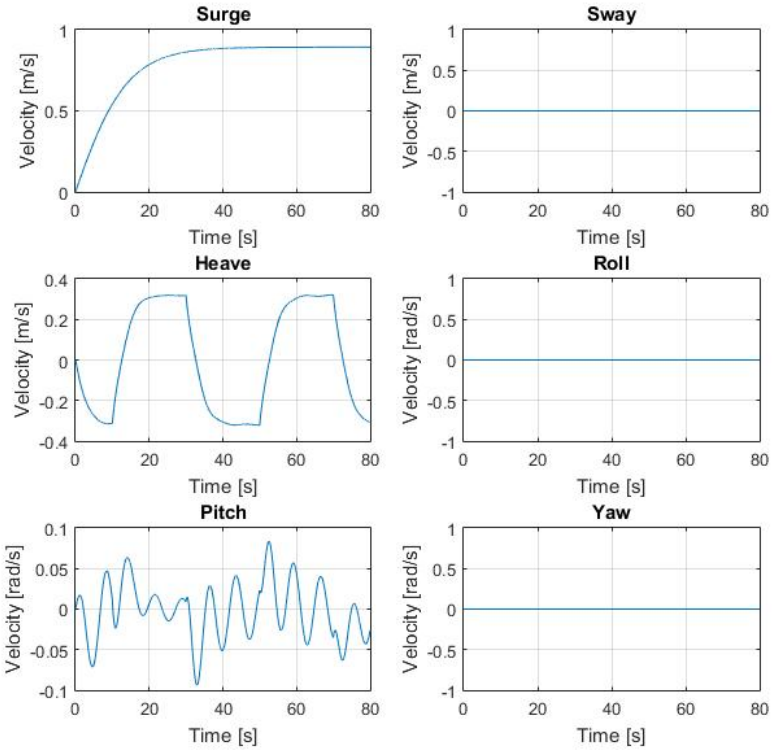

Figure A.4: Complete model velocities for the dive and ascent maneuver (80s simulation).